photonics

MDPI

Review

The Advantages and Disadvantages of Using Structured High-Order but Single Laguerre–Gauss LG_{p0} Laser Beams

Kamel Aït-Ameur

Centre de Recherche sur les Ions, les Matériaux et la Photonique (CIMAP), UMR 6252
CEA-CNRS-ENSICAEN-Université de Caen, 6 Bd Maréchal Juin, CEDEX 4, 14050 Caen, France;
kamel.aitameur@ensicaen.fr

Abstract: Most laser applications are based on the focusing of a Gaussian laser beam (GLB). When the latter is subject to a phase aberration such as the optical Kerr effect (OKE) or spherical aberration (SA), it is recognised that the focusing performance of the GLB is degraded. In this paper, it is demonstrated that high-order radial Laguerre–Gauss LG_{p0} beams are more resilient than the GLB when subject to the OKE or SA. This opens up opportunities to replace with advantages the usual GLB with a high-order LG_{p0} beam for some applications.

Keywords: high-order Laguerre–Gauss modes; rectified Laguerre–Gauss beams; optical tweezers; optical limiting; optical Kerr effect

Citation: Aït-Ameur, K. The Advantages and Disadvantages of Using Structured High-Order but Single Laguerre–Gauss LG_{p0} Laser Beams. *Photonics* **2024**, *11*, 217. https://doi.org/10.3390/photonics11030217

Received: 30 January 2024
Revised: 19 February 2024
Accepted: 20 February 2024
Published: 27 February 2024

1. Introduction

Since the invention of the laser, most people have seen the usual Gaussian laser beam (GLB) as a kind of perfect beam for well-founded reasons based on some parameters characterising its propagation (divergence, M^2 factor, brightness). Generally, the laser cavities are inherently multimode, and a laser oscillation occurring exclusively on the GB is achieved as a result of various strategies. The latter involves either the matching of the pump size for end-pumped solid-state lasers to the size of the desired Gaussian beam in order to maximise the modal overlap [1] or, more simply, by inserting a diaphragm inside the cavity, allowing only the Gaussian mode to oscillate as the fundamental mode [2–4]. The high-order transverse modes have been ignored over a long period of time in such a way that, today, the standard laser beam in most commercial lasers is the GLB. However, we have observed a revived interest in higher-order azimuthal Laguerre–Gaussian modes since the discovery of their orbital angular momentum along the optical axis [5]. High-order azimuthal Laguerre–Gaussian modes have been experimented with in various configurations of optical resonators [6–11]. In contrast, high-order radial Laguerre–Gaussian modes have received little attention of late [12,13]. In the next sections, our study will only deal with high-order radial Laguerre–Gauss LG_{p0} beams made up of a central peak surrounded by p rings of light. The electric field associated with a collimated LG_{p0} beam is given by

$$E_{in}(\rho) = E_0 L_p(2\rho^2/W^2)\exp(-\rho^2/W^2) \quad (1)$$

where L_p is the Laguerre polynomial of order p; W = 1 mm, the width of the collimated Gaussian LG_{00} beam; and ρ is the radial coordinate.

The beam propagation factor of LG_{p0} beams is $M^2 = (2p+1)$, excluding their use for applications requiring high brightness. However, what can be an important drawback can also be an advantage for certain applications of lasers. Indeed, it has been recently shown that LG_{p0} beams are outperforming the Gaussian beam in at least two applications, which are 3-dimensional microfabrication [14] by two-photon polymerisation and in optical tweezers subject to spherical aberration [15]. More precisely, the two above applications involve a rectification of the LG_{p0} beam, which involves transforming the negative rings of

the LG_{p0} beam into a positive one by using a binary diffractive optical element (BDOE) made up of annular zones introducing a phase shift equal to 0 or π, giving rise to a transmittance equal to +1 or -1. The positions of the phase jump from 0 to π or from π to 0, following exactly the zeros of the Laguerre polynomial L_{p}. The main feature of rectified LG_{p0} beams is to give rise to a quasi-Gaussian intensity profile in the focal plane of a focusing lens. The rectification makes a transfer of the energy carried by the rings toward the central part of the focused pattern while keeping the beam propagation factor equal to $(2p + 1)$ [14].

In Section 2, we will examine the effect of particular aberrations (spherical aberration and Kerr effect) on LG_{p0} beams. We will be very surprised by the behaviour of high-order beams. In Section 3, we will consider the spatial properties of "rectified" LG_{p0} beams. In Section 4, we will show that optical tweezers enlightened by an LG_{p0} beam ($p \geq 1$) subject to spherical aberration allow for several increases in the longitudinal and transverse trapping effects compared to the trap enlightened by a pure Gaussian beam. In Section 5, it will be demonstrated that a phase-only binary diffractive optical element is able to transform an LG_{p0} beam into a flat-top or optical bottle beam in the plane of a focusing lens.

2. LG_{p0} Beams Subject to an Aberration

Before proceeding further, it is useful to recall the propagation properties of a pure LG_{p0} beam characterised by an electric field given by Equation (1). Its intensity profile, shown in Figure 1, is made up of a central peak surrounded by p rings of light. It is important to view the wavefront of a collimated radial LG_{p0} beam as alternately concentric out-of-phase rings.

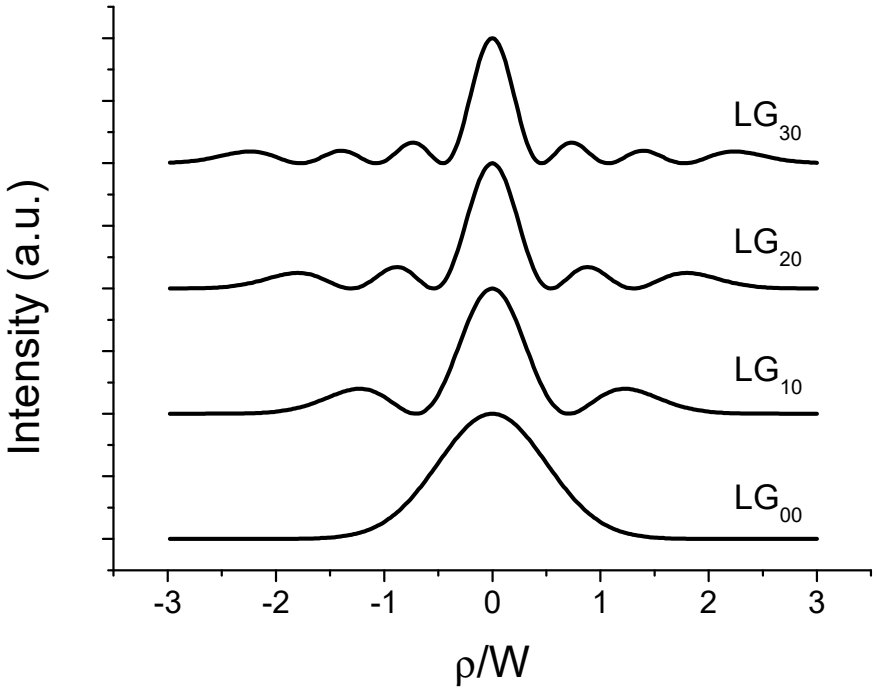

Figure 1. Transverse intensity distribution of the first 4 radial Laguerre–Gauss LG_{p0} beams.

Three fundamental quantities characterising LG_{p0} beams are the Rayleigh range z_R, the beam propagation factor M_p^2, and the longitudinal distribution $W_p(z)$ of the beam width based on the second-order intensity moment [16].

$$z_R = \frac{\pi W_0^2}{\lambda M^2} \tag{2}$$

$$M_p^2 = (2p + 1) \tag{3}$$

$$W_p^2(z) = W_0^2\left[1 + \left(\frac{\lambda M_p^2 z}{\pi W_0^2}\right)^2\right] \quad (4)$$

where the origin $z = 0$ of the longitudinal coordinate is in the beam waist plane of the focused beam and W_0 is the beam waist radius of the LG_{00} beam. It is important to note that the beam width W appearing in Equation (1) has a simple physical meaning only for the fundamental mode LG_{00}, i.e., the width of the Gaussian beam. The beam spreading increases with mode order p so that the beam width W_p in the far-field ($z >> z_R$) is given by

$$W_p = W\sqrt{2p+1} \quad (5)$$

Most uses of laser beams are based on their focusing, as shown in Figure 2, where (PO) stands for a phase object which can be an optical Kerr effect (OKE), spherical aberration (SA) or a binary diffractive optical element (BDOE). These phase objects will be further defined. It is important to keep in mind a particularity of focused LG_{p0} beams giving rise to the same on-axis intensity distribution.

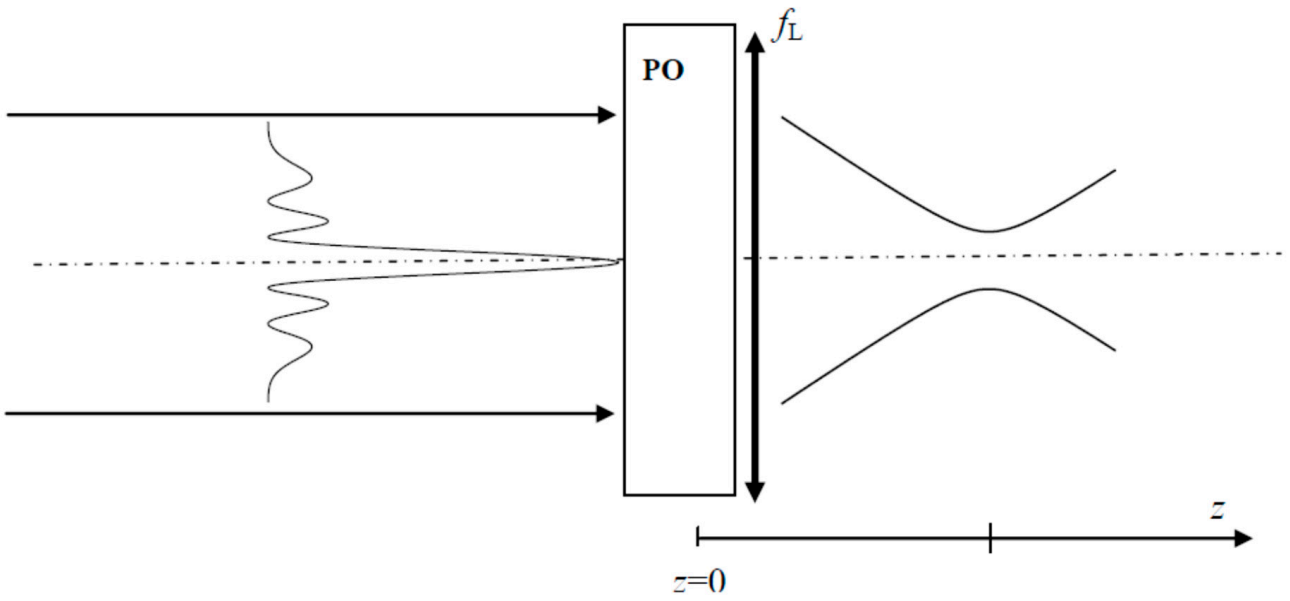

Figure 2. Schematic layout for the focusing of a collimated LG_{p0} beam passing through a phase object (PO) and a lens of focal length f_L. The (PO) can be a Kerr effect, spherical aberration, or a binary diffractive optical element (BDOE).

In the presence of the PO, the incident collimated LG_{p0} beam diffracts, allowing for its restructuring. The diffracted beam through the ensemble (PO + lens) in the plane z is characterised by the electric field $E_d(r,z)$, given by the well-known Fresnel–Kirchhoff formula [17]:

$$E_d(r,z) = \frac{2\pi}{\lambda z}\int_0^\infty \tau(\rho)E_{in}(\rho)\exp[-i\Delta\phi(\rho)]\exp\left[-\frac{i\pi\rho^2}{\lambda}\left(\frac{1}{z}-\frac{1}{f_L}\right)\right]J_0\left[\frac{2\pi}{\lambda z}r.\rho\right]\rho d\rho \quad (6)$$

where r is the radial coordinate in plane z, $k = 2\pi/\lambda$ is the wave number, J_0 is the zero-order Bessel function of the first kind, and $\tau(\rho)$ stands for the transmittance of the phase object (PO). The focusing lens of focal length f_L = 125 mm is assumed to be set quite close to the PO. The diffraction integral given by Equation (6) is calculated numerically by using a FORTRAN 77 routine based on the numerical integrator *dqdag* from the *International Mathematics and Statistical Library* (IMSL). The main characteristics of the diffracted field are as follows:

(i) The intensity distribution $I_d(r,z) = |E_d(r,z)|^2$, which can be split into a longitudinal distribution $I_d(0,z)$ and a transversal distribution $I_d(r,f_L)$ in the plane $z = f_L$.
(ii) The beam propagation factor M_D^2 of the diffracted LG_{p0}. To determine the M_D^2 factor, we need to determine numerically the longitudinal distribution of the width $W_D(z)$ of the diffracted beam based on the second-order intensity moment [18].

$$W_D^2(z) = \frac{2\int_0^\infty I_d(r,z)r^3dr}{\int_0^\infty I_d(r,z)rdr} \tag{7}$$

The calculation of W_D was conducted for 60 values of coordinate z on either side of plane $z = f_L$. From the longitudinal distribution of W_D, we deduced two features. Firstly, the minimum value of W_D, denoted as $W_{D\min}$, and, secondly, the longitudinal position, denoted as $z_{\min}$, where the beam focuses, that is, $W_D = W_{D\min}$. Note that $z_{\min}$ is almost equal to f_L whatever the value of p. The value of the beam propagation factor M_D^2 is defined from a fit of the plot W_D versus z with the following parabola:

$$W_D^2(z) = W_{D\min}^2\left[1 + \left(\frac{M_D^2\lambda(z - z_{\min})}{\pi W_{2\min}}\right)^2\right] \tag{8}$$

Note that the infinite bound in the integral appearing in the numerator of Equation (7) should have a finite value when conducting its numerical evaluation. The choice of the upper integration bound is based on the value of the radial coordinate r, beyond which the intensity $I_d(r)$ could be decreed negligible. Unfortunately, the cubic term r^3 enhances strongly the contribution of the beam wings, although the associated intensity is weak. As a result, the M_D^2 value is very dependent on the upper integration bound and could be overestimated. This is the reason why we preferred a different way of calculating the M^2 factor of the LG_{p0} beam diffracted through a BDOE. This method was based on the decomposition of the diffracted field $E_d(r,z)$ upon a complete basis made up of Laguerre–Gauss functions.

Now let us define the phase aberrations characterising the phase object (PO). The first one is the optical Kerr effect (OKE), for which the complex (PO) transmittance is noted $\tau_1(\rho)$, and the second one is the primary spherical aberration (SA), characterised by its complex transmittance $\tau_2(\rho)$.

2.1. OKE Aberration

The phase object is made up of a nonlinear material having a thickness d and a refractive index $n(\rho) = n_1 + n_2 I_{in}(\rho)$, where $I_{in}(\rho) = |E_{in}(\rho)|^2$ is the incident intensity distribution and $n_1(n_2)$ is the linear (nonlinear) refractive index. As a result, the beam incident on the lens is subject to a phase shift profile $\Delta\phi(\rho)$, given by

$$\Delta\phi(\rho) \approx k n_2 d I_{in}(\rho) \tag{9}$$

where $k = 2\,\pi/\lambda$ and $\lambda = 1064$ nm. The incident collimated beam has a power P and an on-axis intensity $I_0 = 2\,P/(\pi W^2)$, which is unchanged whatever the mode order p. The Kerr phase shift $\Delta\phi(\rho)$ then takes the following form:

$$\Delta\phi(\rho) = \phi_0 \times \left[L_p\left(\frac{2\rho^2}{W^2}\right)\right]^2 \times \exp\left[-\frac{2\rho^2}{W^2}\right] \tag{10}$$

$$\text{with } \phi_0 = \frac{4n_2 P d}{\lambda W^2} \tag{11}$$

ϕ_0 is the nonlinear on-axis phase shift also called the "*breakup integral*" or "*B-integral*" by the community of high-power lasers [19–24]. The complex transmittance of the Kerr phase object is written as $\tau_1(\rho) = \exp[-i\Delta\phi(\rho)]$. The nonlinear phase shift $\Delta\phi(\rho)$ has to be viewed as a phase aberration consisting of defocus and high-order spherical aberrations, which are given in [25] and will not be repeated here. As a result, the defocus term will be responsible for a shift of the best focus toward the lens. In addition to this focus shift, the beam pattern in the geometric focal plane of the linear lens is additionally widened by the spherical aberrations. All these phenomena contribute to the decrease in the on-axis intensity in the focal plane of the focusing lens. Since the nonlinear phase aberration $\Delta\phi(\rho)$ is intensity-dependent, the distortion suffered by the focal spot is also intensity-dependent. Several authors [25–30] have considered this issue by numerical modelling of the diffracted intensity distribution in the geometrical focal plane of the focusing lens when the incident beam is Gaussian, i.e., $p = 0$. In this case, it is observed that the OKE is responsible for a reduction in the focused intensity in the plane $z = f_L$. It is worth noting that since the laser intensity is obviously time-dependent for pulses, light will focus at different locations and, thus, the best focus will "zoom", giving rise to the so-called "focal zoom", which is well described in [31]. As a result, the temporal pulse shape in the focal plane $z = f_L$ is distorted so that it shows a dip near the time corresponding to the peak of the input pulse [19,32]. What was just described in terms of spatiotemporal distortion corresponds to a Gaussian incident beam. The situation is very different for higher-order LG_{p0} beams, as shown in Figure 3, which displays the variations in the on-axis intensity in plane $z = f_L$ versus ϕ_0 [33]. It is seen that the effect of OKE is deleterious when focusing a Gaussian beam since the collapse of $I_d(0, z = f_L)$, the intensity at the centre of the focusing plane, increases greatly with ϕ_0, the nonlinear on-axis phase shift. The plots in Figure 3 show that higher-order LG_{p0} beams are highly resistant to the OKE focal shift so that the intensity $I_d(0, z = f_L)$ remains high despite the nonlinear phase shift. We can see in Figure 3 that the LG_{10} beam is superior to the other LG_{p0} beams in its resistance to the OKE. This is why, in the following sections, particular emphasis will be placed on the LG_{10} beam.

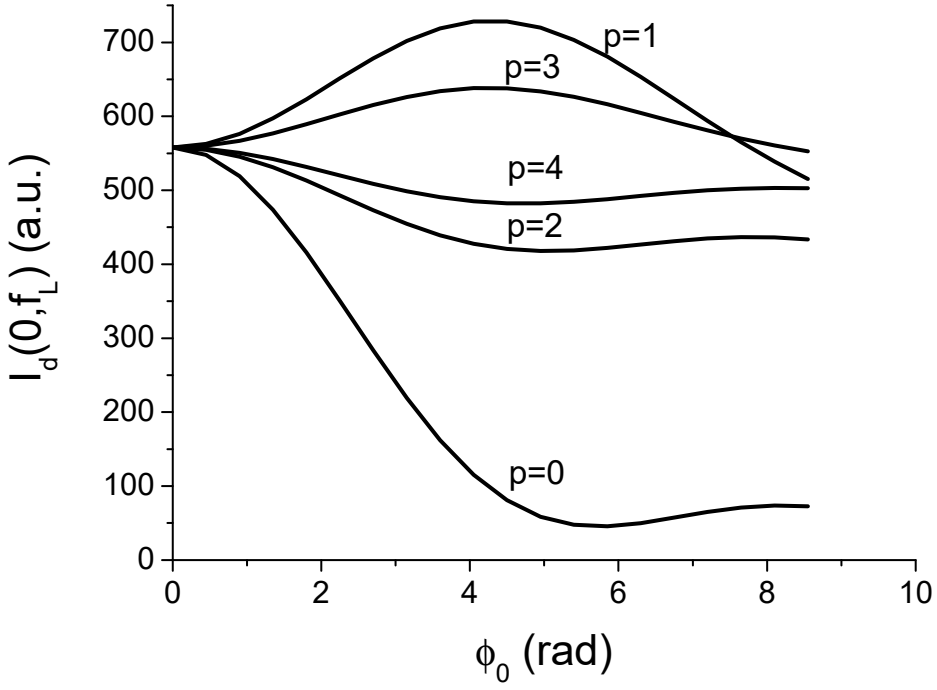

Figure 3. Variations of the on-axis intensity in the focal plane $z = f_L$ versus ϕ_0, the incident on-axis nonlinear phase shift for the first five Laguerre–Gauss beams focused and subject to optical Kerr effect.

Concerning the temporal distortion of the pulse intensity $I_d(0, z = f_L)$ at the beam centre in plane $z = f_L$, due to the OKE, it is much less pronounced for the LG_{10} than for the LG_{00} beam, as shown in Figure 4. The time dependence of the incident pulse has a Gaussian form, i.e., the electric field $E_{in}(\rho)$ has to be multiplied by $\exp[-t^2/\tau^2]$.

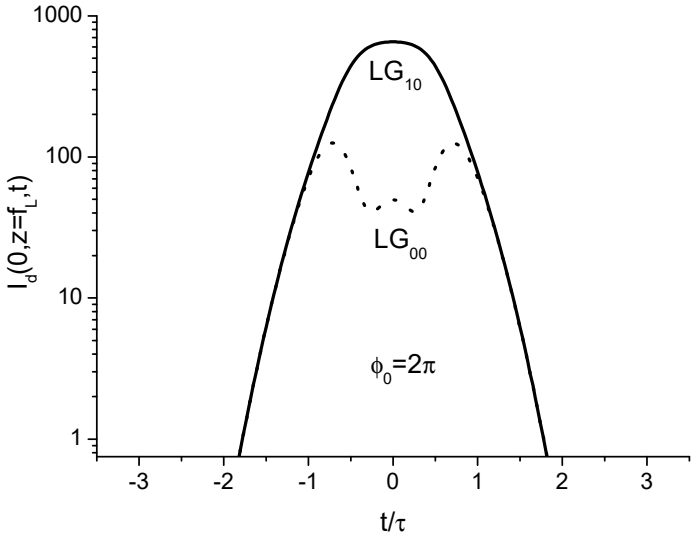

Figure 4. Variations in the focused on-axis intensity of LG_{00} and LG_{10} beams in the focal plane versus the normalised time t/τ, where τ is the pulse duration. The nonlinear on-axis phase shift is $\phi_0 = 2\pi$.

To have a good overview of the degradation of the focused intensity distribution due to the OKE, it is useful to compare the longitudinal distribution of the on-axis intensity $I_d(0, z)$, as shown in Figure 5. The plots in Figures 4 and 5 show that the LG_{10} beam is more resilient than the LG_{00} when both are subject to the optical Kerr effect. This resilience has been discussed in detail in [34]. The superiority, in terms of resilience in space and time, of the LG_{10} beam over the Gaussian beam when subject to the OKE suggests at least two implications: first, it is possible to reduce the protective capacity of optical limiters based on the OKE by enlightening with a LG_{10} beam in place of the usual LG_{00} beam [30] and, second, it could be possible to solve the problem of producing ultra-intense pulses, avoiding the destruction of amplifiers by the phenomenon of beam collapse observed with a Gaussian beam.

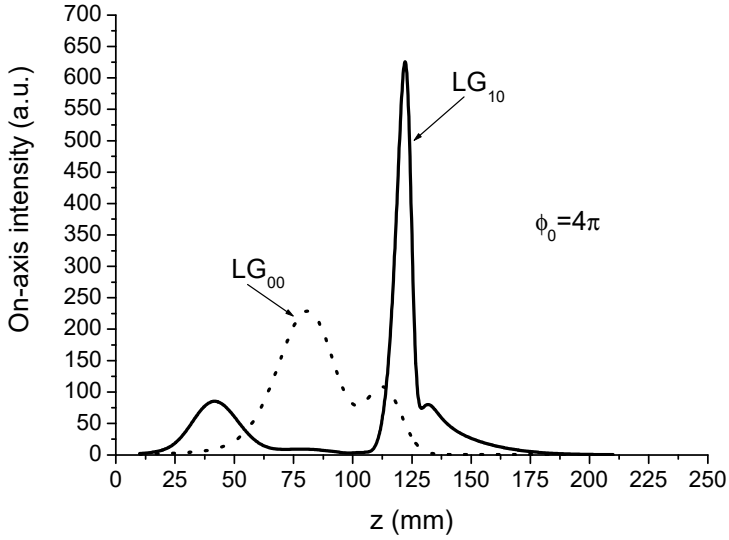

Figure 5. On-axis intensity distribution of focused LG_{00} and LG_{10} beams subject to the optical Kerr effect of $\phi_0 = 4\pi$. The linear lens has a focal length f_L = 125 mm.

In order to clarify expectations on optical power limiters (OPLs) [34–47], the optical limiting device in its simplest form intended to protect some optronic systems is described in Figure 6. The basic elements of the limiting device are a nonlinear Kerr medium of thickness d characterised by a nonlinear refractive index n_2, a linear lens of focal length f_L, and a diaphragm of radius R_D set at a distance L from the ensemble (Kerr medium + lens). Note that it has recently [48] been shown that the position L of the diaphragm is relatively critical since the ensemble (Kerr medium + lens + aperture) acts (i) like a saturable absorber if $L < f_L$, and (ii) is an optical limiting device if $L \geq f_L$.

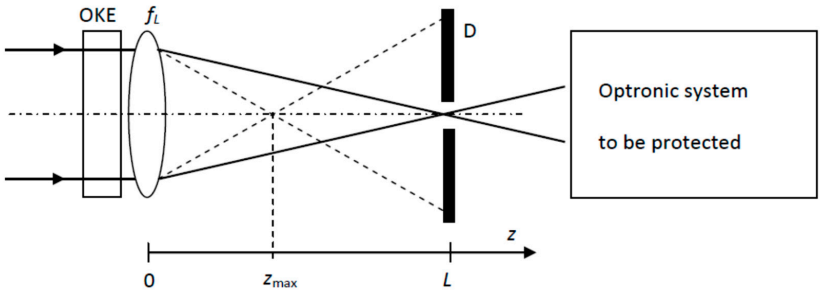

Figure 6. Arrangement for a self-focusing power limiter made up of a nonlinear medium in which the optical Kerr effect (OKE) is induced, with a linear lens of focal length f_L and a diaphragm D of radius R_D. Solid line: low power; dashed line: high power. The best focus is located at $z = f_L$ for low power and $z = z_{max}$ for high power.

It is worth noting that the transmission of a saturable absorber (optical limiter) increases (decreases) with increasing input power. The operating principle of the OPL based on the Kerr effect can be easily understood by considering the Kerr lensing effect, which shifts the best focal point at position z_{max} at high power, while the best focus is located at position z = L at low power. As a result, the longitudinal focal shift from z = L to $z = z_{max}$ enlarges the beam incident on the diaphragm, leading to a reduction in its transmittivity. From the plot in Figure 7, we can then expect that at a high power level, the LG_{10} beam will be less attenuated than the LG_{00} beam [33]. In the case of a pulsed incident laser beam, the transmissivity T of the diaphragm is defined as the ratio of output and input energies. Figure 7 shows the variations of T versus ϕ_0 for LG_{00} and LG_{10} beams. The conclusion is that enlightening an OPL based on the Kerr effect by a LG_{10} laser beam instead of the usual Gaussian beam is a countermeasure since the OPL is almost inefficient in protecting the optical system set after the OPL. Note that the vertical scale in Figure 7 is logarithmic.

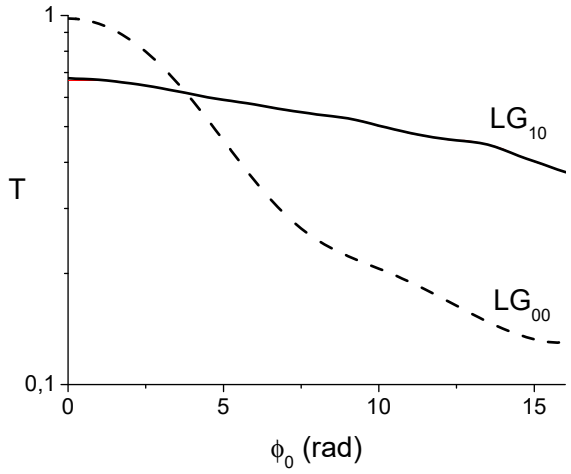

Figure 7. Variations in the dynamic transmittivity T (ratio of energies) of the optical limiter shown in Figure 6 versus the nonlinear on-axis phase shift. Parameters: f_L = 125 mm, W = 1 mm, λ = 1060 nm. The aperture transmission at low power has a value equal to 98%.

The second application concerns the difficulty of laser pulse amplification at a high intensity level in the presence of the Kerr effect occurring in the amplifying medium constituting the amplifier chain. It is worth recalling that, usually, high-power laser chains are made up of a fractioned amplifying medium in order to avoid beam collapse. As seen previously and discussed in detail in [21], the focusing shift due to the Kerr lensing effect is very much less pronounced for the LG_{10} beam than for the LG_{00} beam, and that has an important consequence of laser beam collapse occurring when an intense laser pulse propagates in a bulk optical amplifier. Indeed, it could be expected that the replacement of the usual Gaussian beam by a LG_{10} beam should extend the upper limit of the laser intensity in a high-power laser system, especially for nanosecond pulses. Indeed, for such relatively large pulses, the technique called CPA (chirped pulse amplification) is not as effective as that for femtosecond pulses. For the sake of completeness, it is worth noting that replacing the usual LG_{00} with an LG_{10} beam in the concept of high-power laser chains in the nanosecond regime should require an evaluation of both phenomena known as small- and large-scale self-focusing. This question deserves a close examination that has not yet been conducted in the literature, but which is outside the scope of this paper.

It is known that the beam propagation factor M_D^2 of the beam emerging from the phase object could resume the beam distortion. The variations of M_D^2 versus ϕ_0 are shown in Figure 8 for LG_{00} and LG_{10} beams, and suggest that both beam divergences increase when the nonlinear phase shift ϕ_0 is increased.

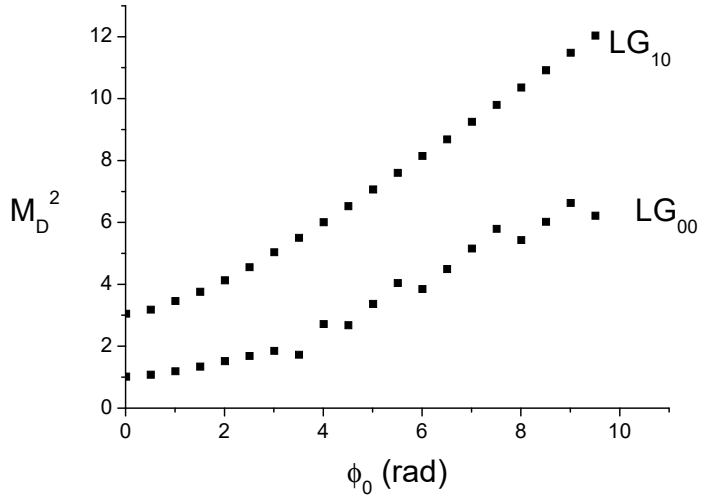

Figure 8. Variations of M_D^2, the beam propagation factor of the LG_{00} and LG_{10} beams passing through a Kerr medium characterised by the nonlinear on-axis phase shift ϕ_0.

For the LG_{00} beam, unsurprisingly, this results in a decrease in the on-axis intensity (see Figure 3) as the beam divergence increases, i.e., ϕ_0 increases. However, for the LG_{10} beam, one observes an unusual behaviour since the on-axis intensity in the plane $z = f_L$ remains high (see Figure 3) when ϕ_0 is increased, while its divergence is increased (see Figure 8).

This unexpected behaviour can be understood in terms of *transverse correlation vanishing* (TCV) due to the presence of a phase aberration. The transverse correlation concept applied to a laser beam means that there is a relation between its centre and its wings: if the beam spreads (shrinks), this results in a decrease (increase) in its on-axis intensity.

Let us first consider the Gaussian beam, viewed as a reference beam in the absence of the focusing lens, in the far-field, namely, at distance z, which is very large compared to its Rayleigh range $z_0 = \pi W_0^2/\lambda$, where W_0 is the beam waist radius. It is easy to show that the relation between the on-axis intensity $I_d(0,z)$ in the far-field and the far-field divergence θ is given by

$$I_d(0,z) \times \theta = K \tag{12}$$

$$\text{With } K = 2P/z^2 \tag{13}$$

where P is the beam power. Equation (12) describes the basic property of a Gaussian beam, which can be formulated as follows.

For a pure Gaussian beam, i.e., without aberration, the far-field on-axis intensity necessarily decreases if the beam divergence is increased, i.e., if the beam is enlarged. Note that this is also a basic property of many other laser beams. However, in the presence of aberration, which is here a Kerr aberration described by Equation (9), this basic property can be changed drastically, and this phenomenon can be described as *transverse correlation vanishing*. It is interesting to compare the TCV associated with the LG_{00} and LG_{10} beams by the use of the figure of merit noted FM and defined by

$$FM = \frac{[K]_{\phi \neq 0}}{[K]_{\phi = 0}} \tag{14}$$

Note that a value of FM close or equal to unity means that the beam fulfils Equation (12), i.e., the far-field on-axis intensity varies relative to the inverse of its divergence angle. The variations of FM versus the nonlinear phase shift ϕ_0 for the LG_{00} and LG_{10} beams are shown in Figure 9. After some algebra, we can express the far-field on-axis intensity $[I_d(0,z)]_{\phi \neq 0}$ of the beam subject to the OKE in terms of the on-axis intensity $[I_d(0,z)]_{\phi=0}$ without aberration as follows:

$$[I_d(0,z)]_{\phi \neq 0} = FM \times \frac{(2p+1)}{M_D^2} \times [I_d(0,z)]_{\phi=0} \tag{15}$$

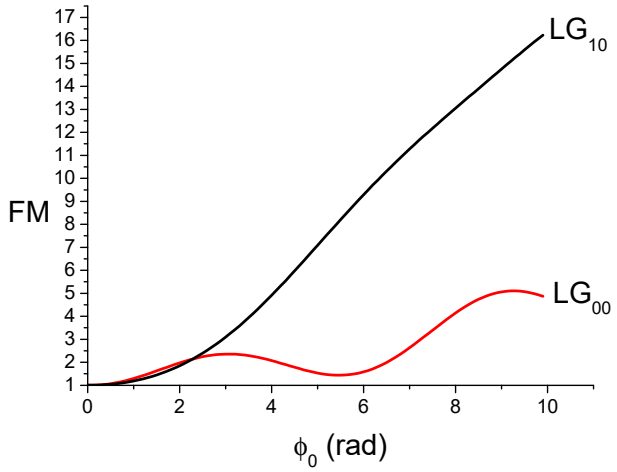

Figure 9. Variations of the figure of merit $FM = [K]_{\phi \neq 0}/[K]_{\phi=0}$ associated with the LG_{00} and LG_{10} beams subject to OKE characterised by the nonlinear phase shift ϕ_0.

For both LG_{00} and LG_{10} beams, the beam propagation factor M_D^2 increases with ϕ_0, as shown in Figure 8, but the increase of FM with ϕ_0 is more important for the LG_{10} beam than for the LG_{00} beam, as shown in Figure 9, so that the on-axis intensity remains high for the LG_{10} beam while it decreases rapidly with ϕ_0 for the LG_{00} beam (see Figure 3). In fact, the diffraction occurring upon the Kerr phase shift produces a transfer of energy from the ring of the LG_{10} beam toward the centre of the beam, maintaining a high intensity in the centre of the focal spot despite the phase aberration. A first conclusion can be drawn from the results of this question, which concerns the quality of laser beam focusing. For a Gaussian beam, the presence of the Kerr effect degrades systematically the focusing quality, i.e., there is intensity reduction in the focal plane. In contrast, it is found that a higher-order transverse Laguerre–Gauss beam, in particular, the LG_{10} beam, is highly resistant to the

Kerr effect, i.e., the intensity in the focal plane remains unchanged until there is at least a nonlinear phase shift of about ten radians.

2.2. Spherical Aberration

The effect of a spherical aberration (SA) on the focusing of a Gaussian beam is well documented in the literature [49–52] while the case of a LG_{p0} beam is less considered or even not studied. The latter is addressed in this Section. Before proceeding, let us define the spherical aberration characterising the PO introduced on the path of the laser beam to be focused, as shown in Figure 2. The complex transmittance τ_2 of the phase object causing the SA is given by

$$\tau_2(\rho) = \exp[-i\phi_{SA}(\rho)] \tag{16}$$

$$\text{with } \phi_{SA}(\rho) = kW_{40}\frac{\rho^4}{\rho_0^4} \tag{17}$$

where $k = 2\pi/\lambda$. W_{40} is the SA coefficient and ρ_0 is the radius of the unit circle, which contains 99% of the incident power. The variations of ρ_0 with the mode order p are given in Table 1.

Table 1. Variations of the radius ρ_0 of the unit circle with the mode order p.

p	0	1	2	3
ρ_0	1.5 W	2.13 W	2.58 W	2.96 W

It is well known that the presence of SA when focusing a Gaussian laser beam degrades the focusing performance, i.e., the intensity in the focal plane is reduced [49–52]. However, for the higher-order Laguerre–Gauss beams ($p \geq 1$), we observe the opposite effect in a similar way to what has been observed with the OKE in the previous section. Indeed, the influence of the SA on the on-axis intensity distribution for $p = 2$, for instance, is shown in Figure 10. It is seen that the SA presence produces an axial shift of the best focus (maximum of $I_d(0, z)$) toward the lens (beyond the plane $z = f_L$) when W_{40} is positive (negative). In addition, one observes a substantial strengthening of the best focus intensity in the presence of SA.

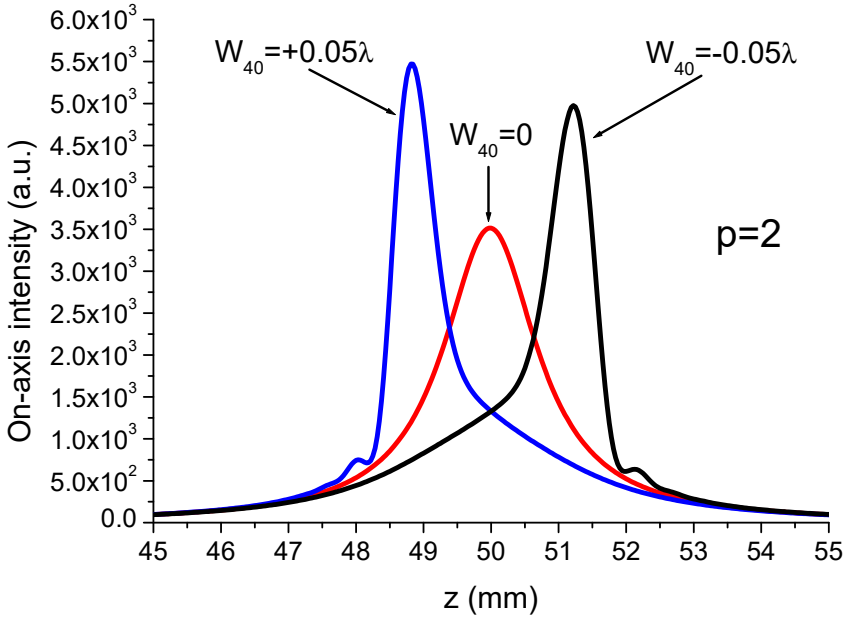

Figure 10. Distribution of the on-axis intensity of an LG_{20} beam passing through a lens of focal length $f_L = 50$ mm and a primary spherical aberration characterised by the coefficient W_{40} equal to -0.05λ, 0, and $+0.05\lambda$.

In order to have a synthetic view of the SA influence on the maximum of the axial intensity, it is convenient to introduce a dimensionless factor Y defined by

$$Y = \frac{[I_d(0,z)]_{\max}^{W_{40}\neq 0}}{[I_d(0,z)]_{\max}^{W_{40}=0}} \tag{18}$$

The meaning of factor Y is that $Y > 1$ ($Y < 1$) indicates that the presence of spherical aberration increases (decreases) the focused intensity. The variations of Y versus W_{40}, for several values of mode order p, are shown in Figure 11. It is worth observing in Figure 11 that Y is less than unity for the LG_{00} beam and greater than one for $p \geq 1$. One can conclude that, in the presence of SA, the focusing of a LG_{p0} beam for $p > 0$ is more efficient than for the GLB.

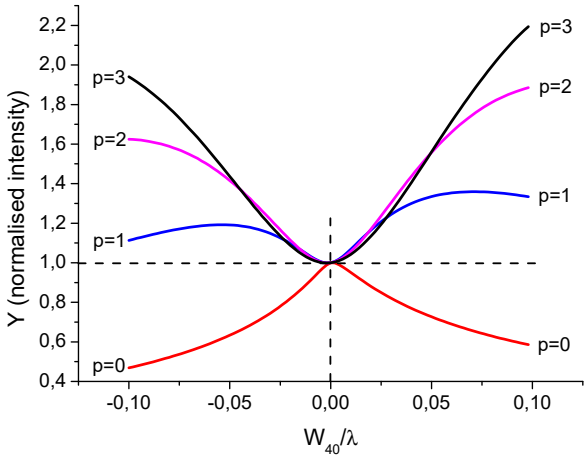

Figure 11. Variation of $Y = [I_d(0,z)]_{\max}^{W_{40}\neq 0} / [I_d(0,z)]_{\max}^{W_{40}=0}$ versus W_{40}/λ, the normalised SA coefficient for different values of p, the mode order.

Another important feature characterising the restructured laser beam is its longitudinal and radial gradient distributions, particularly for the implementation of optical traps (see Appendix A). This point will be expanded on later, but it is useful to consider the influence of W_{40} on the longitudinal intensity gradient for a high-order Laguerre–Gauss beam ($p = 2$ for instance). This is illustrated in Figure 12, which shows clearly that the presence of the spherical aberration enhances the longitudinal intensity gradient.

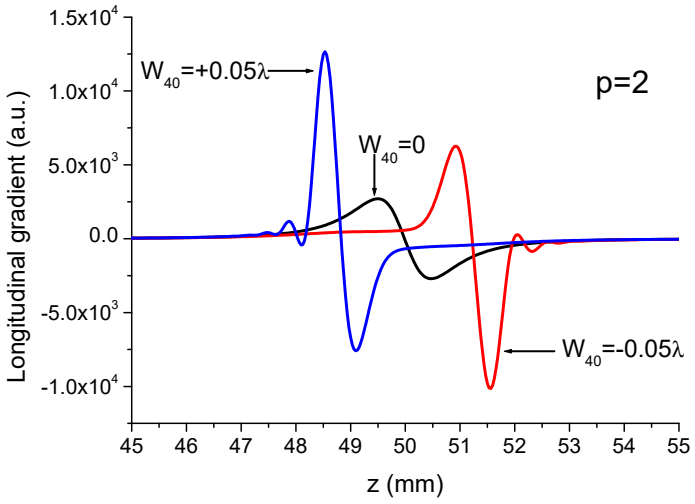

Figure 12. Longitudinal variations of $\hat{z}.\vec{\nabla}_z(I_d(0,z))$, the longitudinal gradient of the intensity $I_d(0,z)$ of an LG_{20} beam passing through a primary spherical aberration characterised by the coefficient W_{40} equal to -0.05λ, 0, and $+0.05\lambda$.

3. The Rectifed LG_{p0} Beams

The concept of "rectification" has been already presented in [14]. The rectification of an LG_{p0} beam for $p \geq 1$ involves introducing a phase object (Figure 2) on its path with the function to convert the alternately out-of-phase rings into a unified phase. The phase object used for achieving the rectification of an LG_{p0} beam is a binary diffractive optical element (BDOE) made up of annular zones introducing a phase shift equal to 0 or π, giving rise to a transmittance equal to +1 or -1 characterised by the transmittance $\tau_3(\rho)$, given by

$$\tau_3(\rho) = \begin{cases} -1 \text{ for } 0 < \rho \leq \rho_1 \\ (-1)^{i+1} \text{ for } \rho_i < \rho \leq \rho_{i+1} \text{ and } (i+1) < p \\ (-1)^{p+1} \text{ for } \rho > \rho_p \end{cases} \quad (19)$$

The position of the phase jumps from 0 to π or from π to 0, following exactly the zeros of the Laguerre polynomial L_p given in Table 2, where the $\rho_i's$ are the p radial positions for which the intensity of the incident beam is null.

Table 2. Roots of Laguerre–Gauss polynomials: $L_p(\rho_i/W) = 0$.

p	Values of Ratio ρ_i/W for the Zeros of the Intensity of the LG_{p0} Mode		
1	0.707106		
2	0.541195	1.306562	
3	0.455946	1.071046	1.773407

The peculiarities of the rectified LG_{p0} beams are that (i) the intensity distribution in plane $z = f_L$ is single-lobed, i.e., the rectification achieves a transfer of energy contained in the rings toward the central peak [15], and (ii) the beam propagation factor is unchanged [14] and remains equal to $M^2 = (2p + 1)$.

The beam propagation factor of rectified LG_{p0} beams is $M^2 = (2p + 1)$, excluding their use for applications requiring high brightness. However, what can be an important drawback can also be an advantage for certain applications of lasers. Indeed, it has been recently shown that LG_{p0} beams are outperforming the Gaussian beam in at least two applications, which are 3-dimensional microfabrication [14] by two-photon polymerisation and in optical tweezers subject to third-order aberration [15]. The main feature of the rectified LG_{p0} beam is to give rise to a quasi-Gaussian intensity profile in the focal plane of a focusing lens, as shown in Figure 13. The rectification makes a transfer of the energy carried by the rings toward the central part of the focused pattern while keeping the beam propagation factor equal to (2p + 1) [14]. Table 3 allows us to compare the fraction of power $\alpha_{LG}(\alpha_R)$ in the central peak of an LG_{p0} beam (rectified LG_{p0}).

Table 3. Power content α_{LG} (α_R) in the central peak of a pure (rectified) Laguerre–Gauss LG_{p0} beam for p varying from 1 to 3. The ratio $\eta = V_G/V_R$ represents the focal volume enhancement factor.

p	α_{LG} (%)	α_R (%)	η
1	26.4	82.6	17
2	15.6	78.5	68
3	11.2	76.3	172

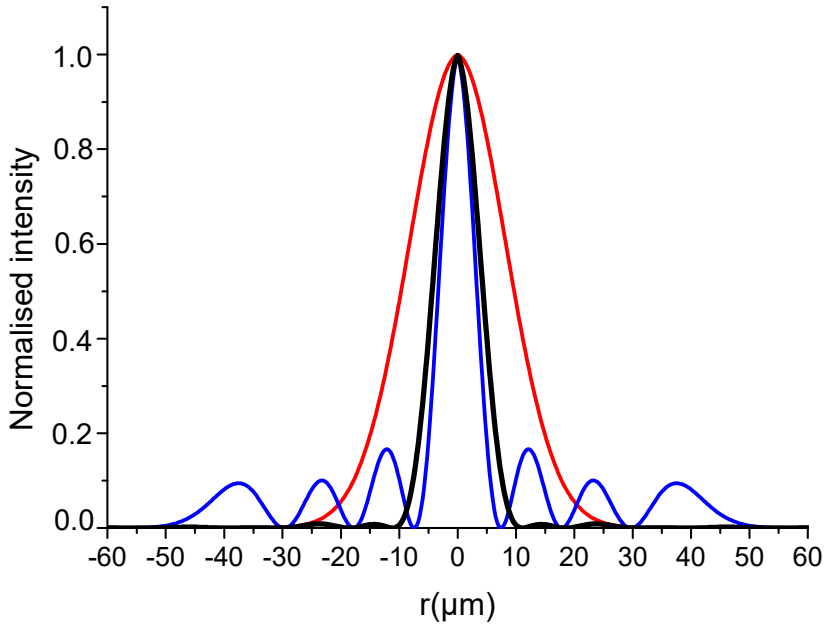

Figure 13. Normalised intensity distribution $I_d(r, f)$ at the focus of a rectified LG_{30} beam (black line). The red (blue) line corresponds to the intensity pattern resulting from the focusing of an LG_{00} (LG_{30}) Gaussian beam.

In order to better understand the benefits of a rectified LG_{p0} beam, there is a need to introduce the concept of focal volume, which defines the volume associated with the focused beam where the intensity can be considered as high. First, let us define the focal volume V_G associated with the Gaussian beam ($p = 0$). It is worth recalling that the focusing of a collimated Gaussian beam of width W incident on a converging lens of focal length f yields a Gaussian focal spot of width W_0, given by

$$W_0 \approx \frac{\lambda f}{\pi W} \tag{20}$$

Note that in Equation (20), it is assumed that the incident Rayleigh distance $(\pi W^2/\lambda)$ is larger than the lens focal length f. Two fundamental quantities characterising the Gaussian beam are necessary. The first one is the Rayleigh range z_R and the second is the longitudinal distribution $W(z)$ of the beam width based on the second-order intensity moment, given by

$$z_R = \frac{\pi W_0^2}{\lambda} \tag{21}$$

$$W^2(z) = W_0^2 \left[1 + \left(\frac{\lambda z}{\pi W_0^2}\right)^2\right] \tag{22}$$

where the origin $z = 0$ of the longitudinal coordinate is in the beam waist plane of the focused beam. The focal volume V_G is defined by the following integral:

$$V_G = \int_{-z_R}^{+z_R} \pi W^2(z) dz \tag{23}$$

It is worth recalling that the focusing of a collimated Gaussian beam of width W incident on a converging lens of focal length f yields a Gaussian focal spot of width W_0, given by

$$W_0 \approx \frac{\lambda f}{\pi W} \tag{24}$$

The associated focal volume is obtained by applying Equation (23):

$$V_G = \frac{\lambda^3 f^4}{\pi^2 W^4} \tag{25}$$

In the same way, it is possible to define a focal volume V_R for the rectified LG_{p0} beam, for which it should be noted that (i) its beam waist size, noted W_f in the plane $z = f_L$, is smaller than that of the focused LG_{00} beam, as shown in Figure 13 for $p = 3$, and (ii) its reduced Rayleigh range is $\pi W_f^2/(\lambda M^2)$. Finally, the reduction in the focal volume by using a rectified LG_{p0} beam in place of the usual LG_{00} beam can be characterised by the following factor:

$$\eta = V_G / V_R \tag{26}$$

The calculation of factor η can be found in [53] and its value is given in Table 3. As pointed out above, in some applications, such as 3-dimensional microfabrication [14] by two-photon polymerisation, for instance, the size of the voxel is of primary importance. A small size allows for the fabrication of small 3-D structures with a high resolution. It may be accepted that the voxel volume is proportional to the focal volume. Consequently, in the case of an incoming Gaussian laser beam, it is seen from Equation (25) that the reduction of V_G requires a short focal length f and a large beam width W. However, tight focusing potentially involves a spherical aberration with the effect of reducing the focused intensity, i.e., increasing the spot size W_0. It is then clear that the use of a laser beam having a poor quality ($M^2 > 1$) can give, after reshaping, rise to a focused quasi-Gaussian pattern. This is a possible solution for reducing the voxel size. For instance, let us consider the case $p = 3$ for which $\eta = 172$ (see Table 3). This means that one can expect an increase in the transverse and longitudinal resolution by a factor of about $(172)^{1/3} \approx 5.5$.

4. Optical Tweezers Enlightened by a Structured LG_{p0} Beam

Usually, optical tweezers are based on the focusing of a Gaussian beam. The essential features of the theory of optical tweezers are recalled in Appendix A, in which two figures of merit are introduced. The first one, noted Z_L, concerns the improvement of the longitudinal trap stability, and the second one, noted Z_R, describes the improvement of the radial gradient of intensity. The objective is to examine if the restructuring of the incident beam in the set-up shown in Figure 2 and the introduction of an adequate phase object (PO) are able to make Z_L and Z_R larger than unity, i.e., improve the performances of the trap.

Before proceeding, it is important to note that all LG_{p0} beams for $p \geq 0$ have the same on-axis intensity distribution. Consequently, replacing the usual Gaussian beam by an LG_{p0} beam cannot improve the longitudinal scattering and gradient forces and thus cannot enhance the longitudinal stability of the trap. However, replacing the usual Gaussian beam by an LG_{p0} beam improves slightly the radial gradient force, as shown in Table 4. These values of ${}^pY_R$ without a PO are identical to those given in Ref. [54]. Now, let us address the crux of the matter by identifying the appropriate phase object (PO) to make Z_L and Z_R larger than one. In fact, this objective is fulfilled by the two phase objects that have been considered above and that are described by Equations (10), (17) and (19).

Table 4. Size of the central lobe of an LG_{p0} beam for $p = 1$ to 3 and the radial enhancement factor.

p	Normalised Radius (ρ/W) of the Central Peak of a Pure LG_{p0} Beam	${}^pY_R$
1	0.7	1.9
2	0.53	2.4
3	0.45	2.9

4.1. The Optical Trap Enlightened by a Rectified LG_{p0} Beam

It is very easy to see that a rectified LG_{p0} beam allows for the improvement of the ratio Z_L. Indeed, intensity and longitudinal gradient are enhanced due to the strong rise in the maximum on-axis intensity owing to the energy transfer from the rings to the central peak. The latter effect is inherent to the rectification process. It has been found that intensity in plane $z = f_L$ of a rectified LG_{p0} beam is enhanced compared with the focusing of a Gaussian beam of the same power by a ratio approximately equal to p [15]. Table 5 shows that factor Z_L is improved, particularly as p is increased [52]. It has been found that the use of a rectified LG_{p0} beam does not improve the radial force of the optical tweezers since ${}^{p}Y_R < 1$ for p = 1 to 3 [54].

Table 5. Variations of ratio Z_L for a rectified LG_{p0} beam.

p	**1**	**2**	**3**
Z_L	2.06	3.37	4.77

4.2. The Optical Trap Enlightened by an LG_{p0} Beam Subject to SA

In Section 2.2, it was recalled that the presence of a positive spherical aberration degrades the focusing performance of a Gaussian beam and enhances the focused intensity of an LG_{p0} beam. Here, we will envisage a spherical aberration that can be positive or negative and consider its influence on ratios Z_L and Z_R. Details of this study can be found in [55], and it will be enough to examine the final results depicted in Figures 14–16. The presence of a spherical aberration, particularly when it is negative, can significantly improve the longitudinal stability of optical tweezers, as shown in Figure 14. Figure 15 confirms that the presence of a positive or negative SA degrades the longitudinal performance of the trap when it is enlightened by a GLB. Concerning the radial force, Figure 16 shows that it is substantially improved, especially for a negative SA, which can be obtained in different ways [55].

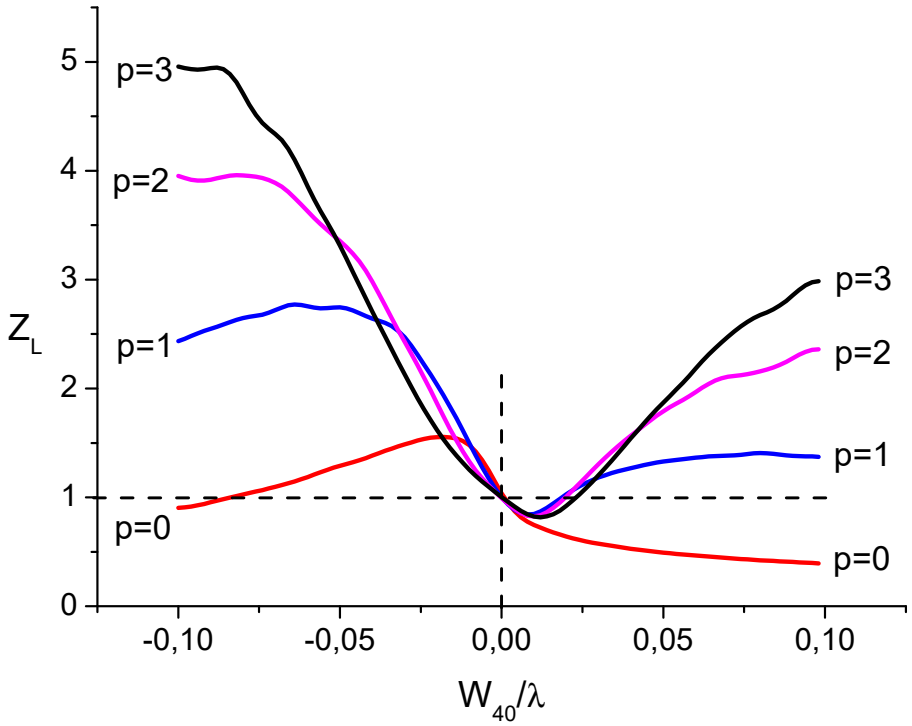

Figure 14. Variations of Z_L versus W_{40}/λ, the normalised primary spherical aberration coefficient. $Z_L > 1$ ($Z_L < 1$) means that the longitudinal stability of the trap is improved (degraded).

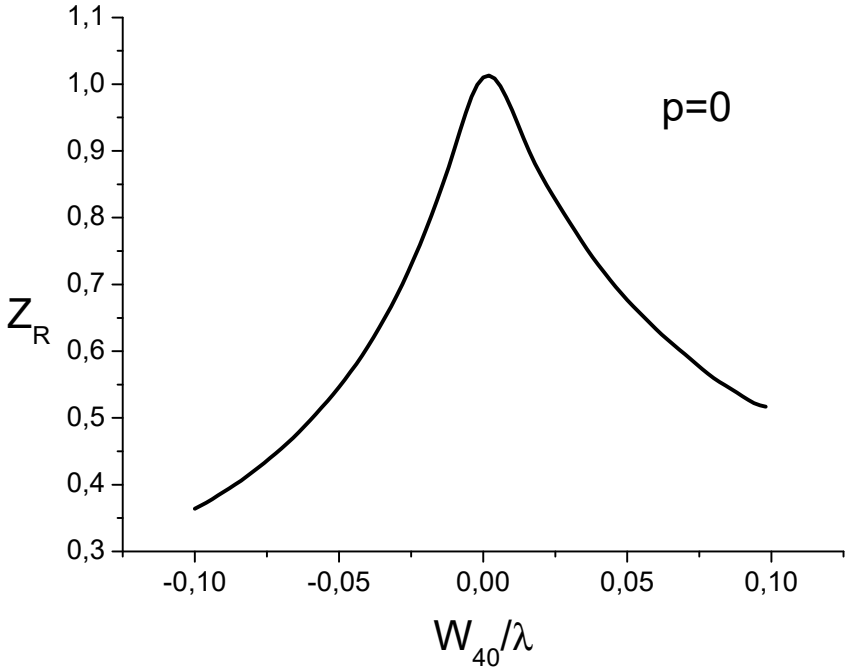

Figure 15. Variations of the radial figure of merit Z_R versus the normalised SA coefficient when the incident beam is a Gaussian beam.

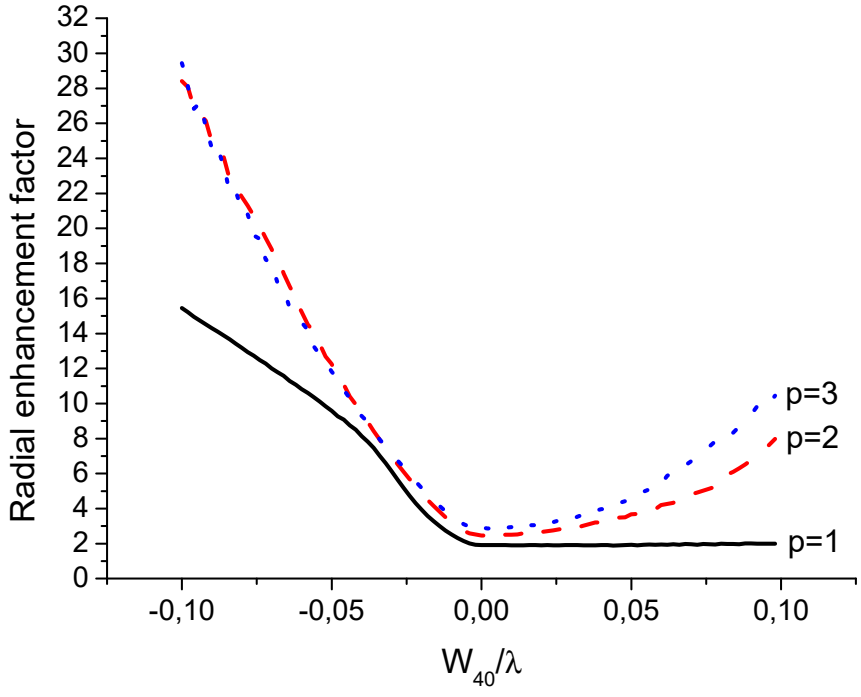

Figure 16. Variations in the radial enhancement factor ${}^{p}Y_R$ versus the normalised SA coefficient for p = 1, 2, and 3.

5. Restructuring an LG_{p0} Beam into a Flat-Top or Optical Bottle Beam

In Section 3, we introduced the concept of "beam rectification", which allows us to generate a quasi-Gaussian intensity profile in the focal plane of a lens focusing a high-order LG_{p0} beam crossing a BDOE defined by Equation (19). Now, in the following section, we will demonstrate that the "partial rectification" of an LG_{p0} beam by using a particular

BDOE—defined hereafter—can give rise to a flat-top or optical bottle beam in the vicinity of the focal plane of a focusing lens.

Before proceeding, let us define the three BDOEs that are considered in the next section. These three devices are a diaphragm, a circular π-plate (CPP), and an annular π-plate (APP), characterised by their transmittances (field ratios) $\tau_D(\rho)$, $\tau_C(\rho)$, and $\tau_A(\rho)$, respectively.

The diaphragm of radius ρ_0 has a transmittance given by

$$\tau_D(\rho) = \begin{cases} 1 \; for \; \rho \leq \rho_0 \\ 0 \; for \; \rho > \rho_0 \end{cases} \tag{27}$$

where ρ is the radial coordinate.

The CPP is a BDOE that introduces a π-phase shift in the central part of the incident beam. It is characterised by the transmittance $\tau_C(\rho)$, expressed as

$$\tau_C(\rho) = \begin{cases} -1 \; for \; \rho \leq \rho_0 \\ +1 \; for \; \rho > \rho_0 \end{cases} \tag{28}$$

The APP is made up of a ring introducing a π-phase shift and its transmittance is

$$\tau_A(\rho) = \begin{cases} -1 \; for \; \rho_1 \leq \rho \leq \rho_2 \\ +1 \; for \; \rho < \rho_1 \; and \; \rho > \rho_2 \end{cases} \tag{29}$$

The CPP and APP are assumed to be made of a transparent material on which is etched a relief of height (or depth) $h = \lambda/[2(n-1)]$, where n is the refractive index of the material and $\lambda = 1064$ nm the wavelength. The height (or depth) of the relief introduces a π-phase shift. Note that, as will be seen later, the BDOE can include two or more dephasing rings.

5.1. Transformation of a Radial Laguerre–Gaussian LG_{p0} Beam into a Flat-Top

As pointed out above, a pure LG_{p0} beam is characterised for $p > 0$ by an electric field given by Equation (1) involving radially a series of p oscillations alternatively positive and negative. For convenience, let us introduce P^+ (P^-), the optical power carried by the positive (negative) part of $E_{in}(\rho)$, and the total power $P_{tot} = P^+ + P^-$. An important parameter characterising the incident beam is η^+, a dimensionless quantity defined as

$$\eta^+ = \frac{P^+}{P_{tot}} \tag{30}$$

The pertinence of parameter η^+ has been recently demonstrated [15,56]. Indeed, it was found that when η^+ is close to 0.96, the far-field distribution is made up of a flat-top intensity profile [56]. In contrast, when η^+ is in the range of 67% to 74%, the far-field is a hollow beam or, more precisely, an optical bottle beam [57].

In the next section, we will demonstrate that the implementation of the η^+ concept allows for the reshaping of the LG_{p0} beam, for $p \geq 1$, into a flat-top (FT) or optical bottle beam (OBB). Before proceeding, let us consider the value of η^+ associated with a pure LG_{p0} beam given in Table 6.

Table 6. Fraction of power carried by the negative rings potentially subject to rectification and ratio η^+ for a pure LG_{p0} beam.

p	**0**	**1**	**2**	**3**	**4**	**5**
Central peak (positive)	100%	26.4%	15.6%	11.1%	8.6%	7.1%
Ring #1 (negative)		73.6%	23.5%	15.3%	11.5%	9.24%
Ring #3 (negative)				53.7%	17.5%	11.8%
Ring #5 (negative)						45.7%
η+ (pure LG_{p0})	100%	26.4%	75.9%	30.9%	70.8%	33.2%

Recently, it has been shown [56] that an LG_{10} beam can be transformed into an FT profile in the focal plane of a focusing lens by increasing its η^+ value from 26.4% to 93.4% just by partially truncating the negative ring by using a diaphragm that gives rise to a loss of about 72%. In the next section, it will be shown that a LG_{10} beam can be transformed into an FT intensity profile in the far-field region by converting a part of the negative ring into a positive value without loss. This is achieved by a transparent phase-only diffractive optical element such as CPP or APP described above. In addition, we will examine if the η^+ concept could be applied to higher values of p in order to generate a flat-top intensity profile after focusing. For the study of the partial rectification of an LG_{p0} beam in order to generate an FT profile in the focal plane of a converging lens, we will consider the optical layout given in Figure 2, where the phase object (PO) is replaced by one of the BDOEs defined in Equations (27)–(29). In the following, the calculation of the diffracted field through the ensemble (BDOE + lens) in plane z is obtained by using the well-known Fresnel–Kirchhoff formula given by Equation (6).

Before proceeding, it is important to note that the ability of transforming an LG_{p0} beam into a flat-top intensity profile by using a phase-only BDOE achieving a partial rectification is very different depending on the parity of the beam order p. As said above, the position of the phase jumps from 0 to π and from π to 0, characterising the phase-only BDOE, in order to achieve the partial rectification of a ring light, with some connected to the position of the zeros of the Laguerre polynomials L_p. The latter are given in Table 2.

5.1.1. Reshaping of Odd LG_{p0} Beams: LG_{10}, LG_{30}, LG_{50}

(a) LG_{10} beam

As given in Table 6, the value of η^+ for the free LG_{10} beam is equal to 26.4% and must be modified to about 90% (with reference to [56]) in order to obtain a flat-top profile in the focal plane of a converging lens. For this, we planned to partially rectify the negative ring by using as a BDOE an annular π-plate (APP) defined by Equation (29), where $(\rho_1/W) = Y_A$ and $(\rho_2/W) = Y_B$. The value of Y_A was fixed to 0.707106 (zero of LG_{10} beam intensity) and Y_B was variable. To find the right value of Y_B, allowing for the transformation of the LG_{10} beam into an FT intensity profile, we needed to "rectify" (90−26.4) = 63.6% of the ring power content. As a consequence, the circle of radius $Y_B W$ contained 90% of the total power P_{tot}, and the value of Y_B could be deduced from the variations of the normalised power $P(\rho)/P_{tot}$ contained in the circle of normalised radius $Y = \rho/W$, plotted in Figure 17. The extrapolated value of Y for which $[P(\rho)/P_{tot}] = 90\%$ was Y_B = 1.7. Then, we needed to check that the intensity distribution $I_d(r, z = f_L)$ was effectively a flat-top.

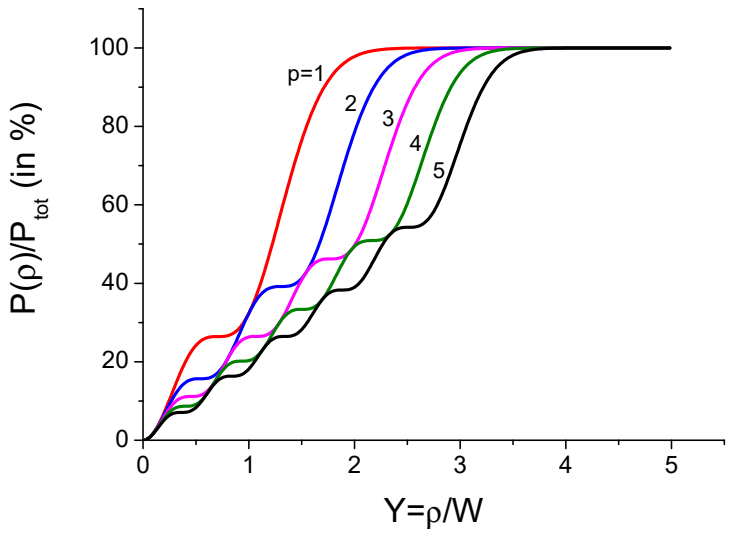

Figure 17. Variations of the normalised power $P(\rho)/P_{tot}$ contained in the circle of radius $\rho = YW$.

The result is shown in Figure 18, which confirms the achievement of an FT profile. The diffracted beam had a beam propagation factor found to be $M_D^2 = 4.6$. We could also determine as previously the value of Y_B giving rise to an optical bottle beam (OBB). For this, as said previously, the parameter η^+ had to be in the range of 67% to 74%. As a result, the partial rectification of the ring needed to be in the range of 67−26.4% to 74−26.4%, namely, 40.6% to 47.6%. From the plot in Figure 17 for $p = 1$, we extrapolated the value of Y_B, which was in the range of 1.4 to 1.47.

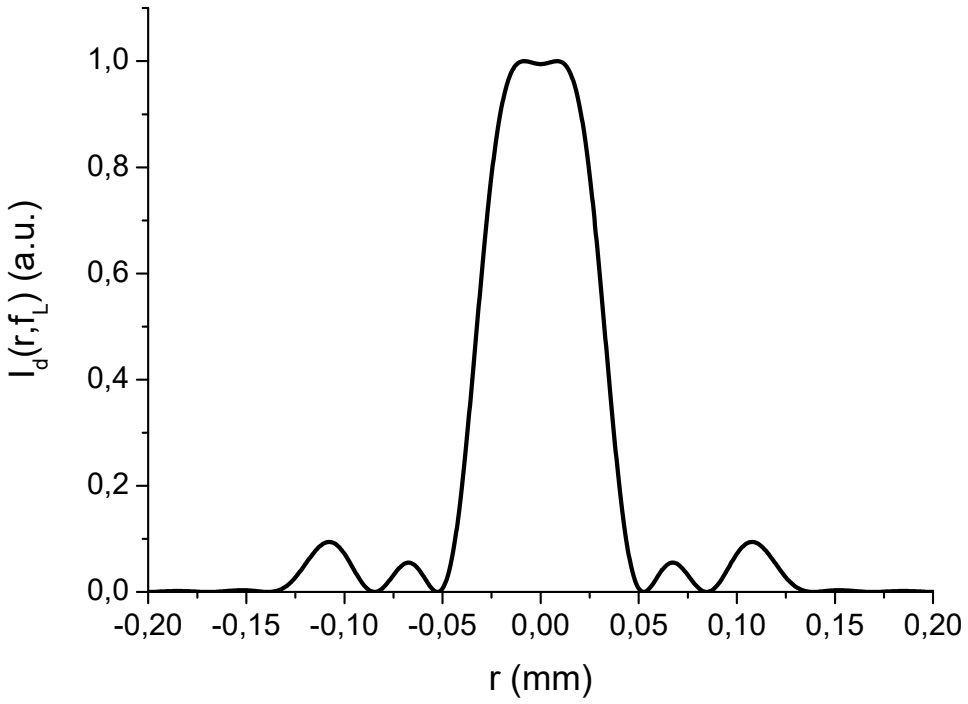

Figure 18. Normalised intensity distribution in the focal plane of a converging lens of focal length $f_L = 125$ mm when the incident LG_{10} beam with $W = 1$ mm was partially rectified by a π-dephasing ring bounded by the circles of normalised radius $Y_A = 0.707$ and $Y_B = 1.7$. The beam propagation factor of the reshaped beam was found to be $M_D^2 = 4.6$.

The result shown in Figure 19 displays the expected hollow intensity profile with a beam propagation factor of $M_D^2 = 5.4$. However, in order to confirm that we are dealing with an OBB, we have to plot the on-axis intensity distribution, namely, $I_d(0, z)$ versus z. The result is shown in Figure 20, which effectively confirms that the reshaping of the LG_{10} beam generates for $Y_B = 1.4$ an OBB "closed" by the two longitudinal peaks of intensity playing the symbolic role of the "cork" and "bottom" of the light bottle. It is worth remembering that an OBB consists of a dark (minimal intensity) region surrounded in all directions by regions of higher intensity. Such OBBs are very useful for the trapping of cold neutral atoms [58–60] or metal nanoparticles [61–67]. It is interesting to compare the OBB length $\Delta z = 4.3$ mm, which represents the distance between the two intensity peaks appearing in Figure 20, to the Rayleigh range z_R of the pure focused LG_{10} beam (without a BDOE). The distance z_R (for $p = 1$) is expressed as a function of the beam waist size W_0 of the focused collimated Gaussian beam of width $W = 1$ mm:

$$z_R = \frac{\pi W_0^2}{(2p+1)\lambda} = 5.3 \text{ mm} \tag{31}$$

$$\text{With } W_0 = \lambda f_L/(\pi W) = 42 \text{ µm} \tag{32}$$

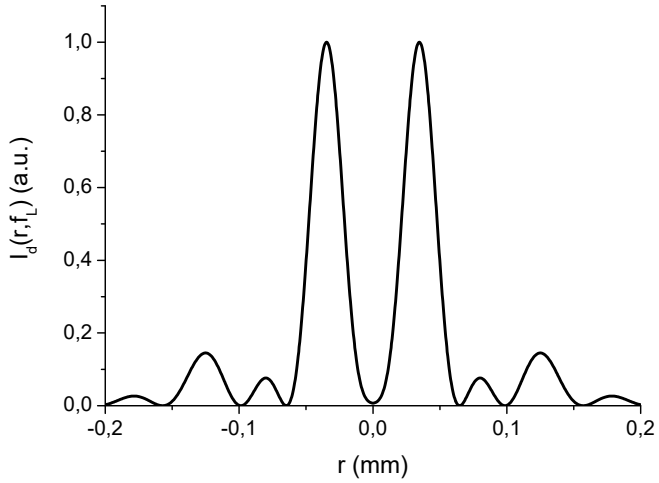

Figure 19. Normalised intensity distribution in the focal plane of a converging lens of focal length f_L = 125 mm when the incident LG_{10} beam with W = 1 mm was partially rectified by a π-dephasing ring bounded by the circles of normalised radius Y_A = 0.707 and Y_B = 1.4. The beam propagation factor of the reshaped beam was found to be $M_D^2 = 5.4$.

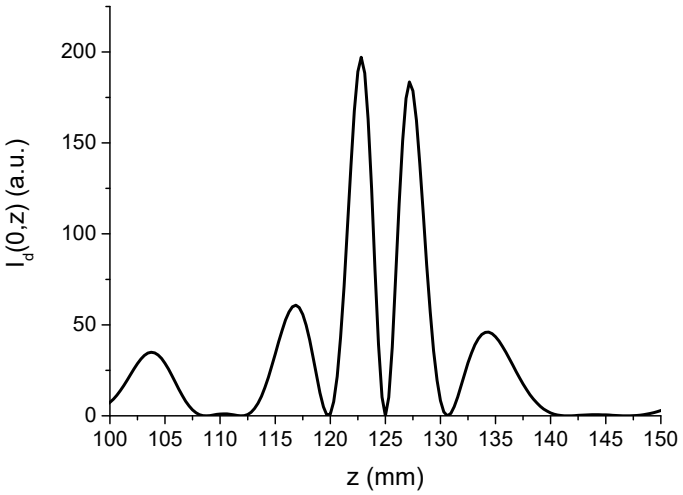

Figure 20. On-axis intensity distribution $I_d(0,z)$ for an LG_{10} beam partially rectified by an annular phase plate (Y_A = 0.707 and Y_B = 1.4) for $f_L = 125$ mm and W = 1 mm.

As a result, the OBB length was found to be $\Delta z = 0.8\, z_R$, while the same reshaping of the LG_{10} beam achieved by using a diaphragm gave an OBB length of $\Delta z = 6.6\, z_R$ [57].

(b) LG_{30} beam

A close look at Table 6 shows that the rectification of a single ring was not enough to increase η^+ from 30.9% (pure LG_{30} beam) to the range of 67% (OBB) to 90% (FT). Consequently, it was necessary to rectify fully Ring #1 and partially Ring #3 so that the adequate BDOE was a double annular π-plate (APP) made up of two π-dephasing rings, bounded by the circles of normalised radius Y_A = 0.455 and Y_B = 1.071 for the first ring and the circles of normalised radius Y_C = 1.77 and Y_D = variable for the second ring. In order to reshape the LG_{30} beam into an OBB, η^+ needed to be close to 67%, and this could be achieved if 20.8% of Ring #3 were rectified. As conducted previously for the LG_{10} beam, we deduced Y_D = 2.26 from Figure 17 for p = 3. The value expected for Y_D in order to obtain an FT profile was Y_D = 2.58. The intensity profile $I_d(r, z = f_L)$ showed that the best value of Y_D to obtain the best OBB (FT) was 2.1 (2.45), as shown in Figure 21a,b. Both beams had a beam propagation factor of $M_D^2 = 10.8$ instead of a beam propagation factor of $M_D^2 = 7$ associated with the incident beam.

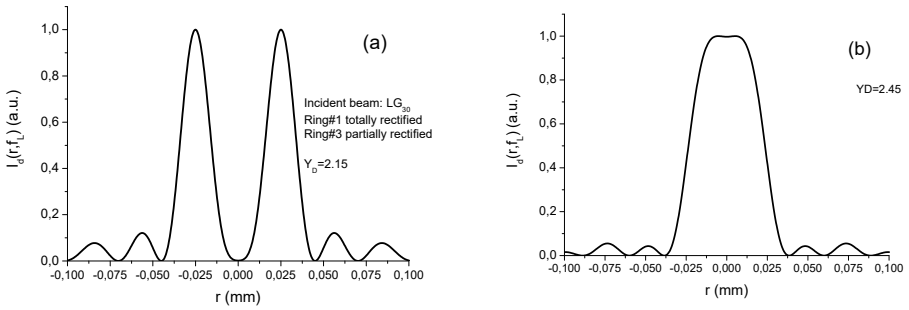

Figure 21. Normalised intensity distribution in the focal plane of a converging lens of focal length f_L = 125 mm when the incident LG_{30} beam with W = 1 mm had Ring #1 totally rectified and Ring #3 partially rectified. The BDOE took the form of a double APP. The second π-dephasing ring was bounded by the circles of normalised radius Y_D: (**a**) for $Y_D = 2.1$, the intensity profile was an OBB with $M_D^2 = 10.8$ and (**b**) for $Y_D = 2.45$, we obtained a flat-top profile with $M_D^2 = 10.8$.

(c) LG_{50} beam

The LG_{50} beam had three positive and three negative zones and was characterised by $\eta^+ = 33.2\%$. Consequently, it is seen from Table 6 that the generation of an OBB was possible with a single APP rectifying partially Ring #5. The single APP was bounded by the circles of normalised radius Y_A = 2.51 (fifth zero of intensity) and Y_B = 3.18, determined from Figure 17. By doing this, the BDOE rectified 67−33.2% = 33.8% of the last ring, and the best hollow intensity profile shown in Figure 22 was obtained for Y_B = 2.95 instead of the expected value Y_B = 3.18. The plot in Figure 22 shows that the quality of the hollow profile was bad because of the existence of numerous rings. It was found that the partial rectification of Ring #5 did not allow the generation of an FT profile, whatever the value of Y_B.

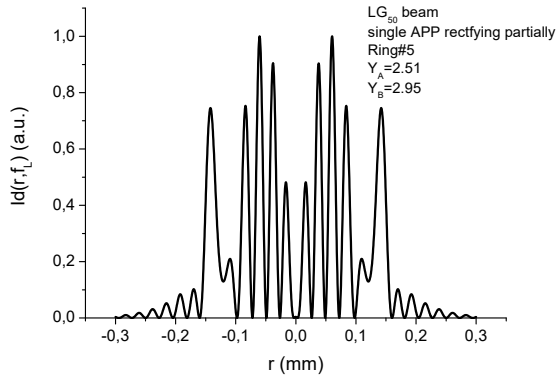

Figure 22. Normalised intensity distribution in the focal plane of a converging lens of focal length f_L = 125 mm when the incident LG_{50} beam with W = 1 mm had Ring #5 partially rectified by a π-dephasing ring bounded by the circles of normalised radius $Y_A = 2.51$ and $Y_B = 2.95$.

The second possibility allowing for the generation of an OBB or FT was the use of a double APP rectifying totally Ring #3 and partially Ring #5. In accordance with Table 6 and Figure 17, the needed BDOE was made up of two π-dephasing rings bounded by the circles of normalised radius Y_A = 1.34 and Y_B = 1.88 for Ring #3 and the circles of radius Y_C = 2.51 and Y_D for the second ring, having different values depending on the desired intensity profile, i.e., OBB or FT. Without repeating what has been explained above, we expected an OBB if $Y_D = 3$ and an FT profile if Y_D = 3.5. Just as before, we found from the numerical calculation that the OBB and FT profile were obtained for different values of Y_D. In Figure 23a,b, it is seen that the intensity profile was an OBB (FT) for Y_D = 2.6 (Y_D = 3.05). The beam propagation factor was found to be $M_D^2 = 14.5$ ($M_D^2 = 15.5$) for the OBB (FT) profile instead of the beam propagation factor $M_D^2 = 11$ associated with the incident beam.

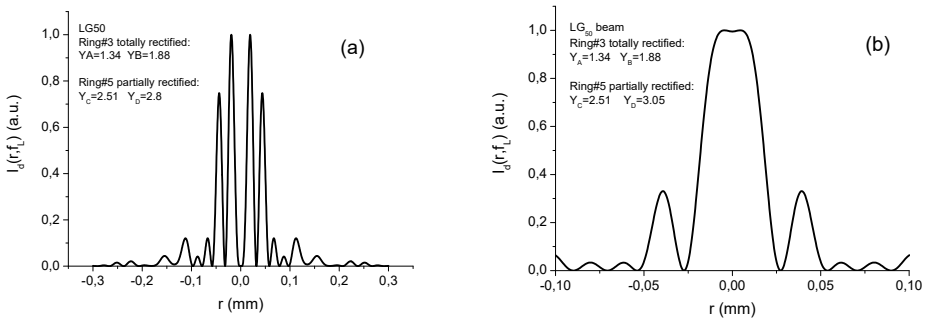

Figure 23. Normalised intensity distribution in the focal plane of a converging lens of focal length f_L = 125 mm when the incident LG_{50} beam with W = 1 mm had Ring #3 totally rectified and Ring #5 partially rectified. The BDOE took the form of a double APP. The second π-dephasing ring was bounded by the circles of normalised radius Y_D: (**a**) for Y_D = 2.8, the intensity profile was an OBB with $M_D^2 = 14.5$ and (**b**) for Y_D = 3.05, we obtained a flat-top profile with $M_D^2 = 15.5$.

5.1.2. Reshaping of Even LG_{p0} Beams: LG_{20}, LG_{40}

By following the procedure detailed above for odd LG_{p0} beams, we modified the value of η^+ of LG_{20} and LG_{40} beams by using a single APP or double APP without reaching the expected FT and OBB profiles in plane $z = f_L$. In addition, no conspicuous beam reshaping was observed when the geometry of the single or double APP was varied. It must be concluded, without identifying the reasons for such behaviour, that the reshaping of an LG_{p0} beam into an FT or OBB profile by using a binary phase-only DOE is only possible for odd order p.

In summary, we have demonstrated that the intensity profile in the focal plane can be a flat-top (FT) or an optical bottle beam (OBB), provided that η^+ has an adequate value 96% or 67 to 74%. The adjustment of parameter η^+ was made using a phase-only binary diffractive optical element (BDOE) introducing a π-phase shift realising an operation of partial rectification of the negative part of the LG_{p0} beam. The wording *rectification* means that the negative electric field is transformed into a positive electric field. The resulting restructuring of the LG_{p0} beam by the partial rectification led to an FT or an OBB, but only for odd order p. The phase-only BDOE could be made of a transparent material on which was etched (one etching level) a relief introducing the π-phase shift over the adequate circular areas calculated to obtain the desired η^+. The use of such a device has at least two main advantages, which are, firstly, low cost compared to a spatial light modulator [68] or deformable mirror [69] and, secondly, the ability to sustain high light intensities without damage.

6. Conclusions

It is important to note that the high-order transverse mode has been disqualified from the applications of laser beams since the 1960s because it is more divergent and less bright that the Gaussian laser beam (LG_{00} beam). Since that time, the Gaussian laser beam has been put on a pedestal, but, from the 1990s, high-order modes have gained renewed interest. We can mention the higher-order azimuthal Laguerre–Gauss modes since the discovery that they possess well-defined orbital angular momentum along the optical axis for non-zero values of the azimuthal order [5]. In contrast, high-order radial Laguerre–Gaussian beams have received little attention as of late [70]. In this review, we wanted to emphasize some very promising properties of restructured high-order radial Laguerre–Gauss beams. It would be desirable to experiment with optical trapping with restructured LG_{p0} beams (by using OKE, SA, or rectification) in order to benefit from improved trapping performances. However, the first step should be to produce a LG_{p0} beam since commercial lasers deliver mainly Gaussian beams. This can be achieved by inserting inside the laser cavity a mask made up of absorbing rings [13] or a BDOE such as that described by Equation (19) [9,10,70]. Another possibility could be to transform a Gaussian beam into a LG_{p0} beam by using an SLM and then carrying out efficient amplification [71]. It will be interesting to extend the study of intensity and

gradient distributions with other structured laser beams such as Bessel–Gauss beams and generalised Laguerre–Gauss beams, which have attractive properties [72]. Finally, it would be interesting to examine if restructured LG_{p0} beams can be more performant than GLBs for applications other than those considered in this paper [73].

Funding: This research received no external funding.

Institutional Review Board Statement: Not applicable.

Informed Consent Statement: Not applicable.

Data Availability Statement: Data are contained within the article.

Acknowledgments: I would like to thank my collaborators, M. Fromager, E. Cagniot, A. Hasnaoui, A. Harfouche, S. Haddadi, D. Naidoo, S. Ngcobo, and A. Forbes, who have helped me for many years in the study of many aspects of the structuring of radial high-order Laguerre–Gauss beams.

Conflicts of Interest: The author declares no conflicts of interest.

Appendix A

Optical tweezers are today an indispensable tool for manipulating non-invasively small particles. Initial work on the subject began in the 1970s by the pioneer Arthur Ashkin, and remains a major challenge of intensive research. The latter corresponds to the case where we are dealing with a spherical dielectric particle of radius a much smaller than the laser wavelength ($a << \lambda$). In this context, the trapped particle is treated as a point-induced electric dipole interacting with the electromagnetic field associated with the focused laser beam. The theory of optical tweezers is described in detail in [74–79], and the essential elements are briefly recalled below. The experimental setup allowing for the implementation of usual optical tweezers involves a Gaussian laser beam and a focusing lens, as shown in Figure A1.

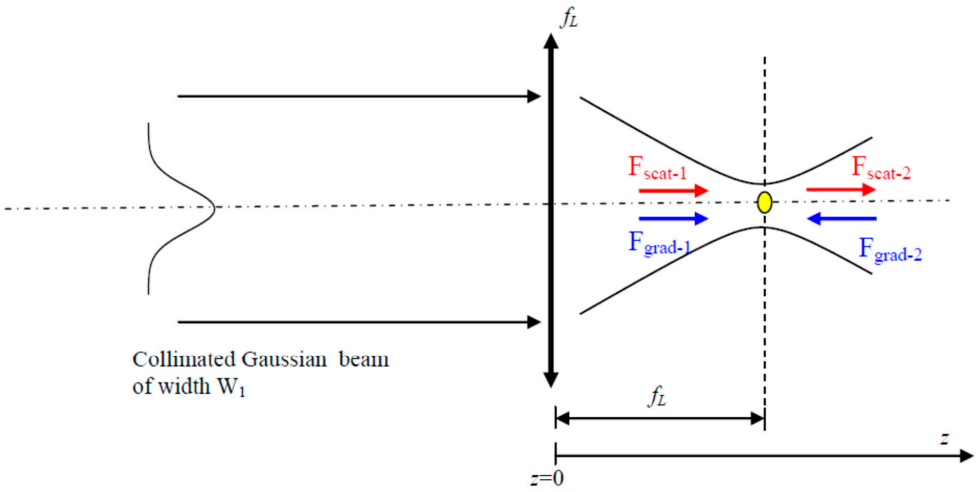

Figure A1. Optical trap set-up showing the scattering (in red) and gradient (in blue) longitudinal forces. The focusing lens has a focal length f_L.

The trapping of the small dielectric particle involves two longitudinal forces, as shown in Figure A1. The first force is a gradient force $\vec{F}_{grad}$ proportional to the longitudinal gradient of the distribution of intensity. The second one is the scattering force $\vec{F}_{scat}$ proportional to the longitudinal distribution of intensity. These two forces are given by

$$\vec{F}_{grad} = \frac{4\pi a^3}{c}\left[\frac{m^2-1}{m^2+2}\right]\vec{\nabla}_z I_d(r,z) \quad \text{(A1)}$$

$$\vec{F}_{scat} = \frac{128\pi^5 n_m a^6}{3c\lambda^4}\left[\frac{m^2-1}{m^2+2}\right]^2 I_d(r,z)\hat{z} \tag{A2}$$

where $m = n_p/n_m$ is the ratio of the refractive index of the particle n_p and the surrounding medium n_m. The quantity $I_d(r,z)$ is the intensity distribution beyond the focusing lens, where r is the radial coordinate in plane z. In Equation (A1), the gradient ($\vec{\nabla}$) operator has longitudinal and radial components giving rise to a longitudinal gradient force and a radial gradient force. Note that in Figure A1, the two forces ($\vec{F}_{grad-1}$ and $\vec{F}_{scat-1}$) are noted in the region $z < f_L$ and ($\vec{F}_{grad-2}$ and $\vec{F}_{scat-2}$) are noted in the region $z > f_L$. In the next section, we will focus on the longitudinal components (r = 0) of the two forces $\vec{F}_{scat}$ and $\vec{F}_{grad}$. In cases in which the incident laser beam is Gaussian, the on-axis intensity distribution $I_d(0,z)$ is symmetric with respect to the plane $z = f_L$. Consequently, in the case of Gaussian illumination, we have $\vec{F}_{scat-1} = \vec{F}_{scat-2}$ and $\vec{F}_{grad-2} = -\vec{F}_{grad-1}$.

The condition that must be met in order to trap the particle is to fulfil the inequality $\left|F_{grad-2}\right| > |F_{scat-2}|$, where F_{grad} (F_{scat}) is the projection of $\vec{F}_{grad}$ ($\vec{F}_{scat}$) in the $\hat{z}$ direction. The ratio F_{grad}/F_{scat} is expressed as follows:

$$\frac{F_{grad}}{F_{scat}} = K\frac{\hat{z}\vec{\nabla}_z\{I_d(r,z)\}}{I_d(r,z)} \tag{A3}$$

$$\text{with } K = \frac{3\lambda^4}{32\pi^4 n_m a^3}\left[\frac{m^2+2}{m^2-1}\right] \tag{A4}$$

The objective is to set a phase object (PO) on the path of the incident beam (Figure 2), achieving a restructuring of the laser beam in order to improve the performance of the trap. For this, we define dimensionless factors characterising the longitudinal and radial force improvements. For convenience, in the next section, we will express the stability of the optical trap by a relevant quantity noted R, which is proportional to the ratio of the backward axial gradient and the forward scattering forces [15]:

$$R = \frac{-K\hat{z}.\left[\vec{\nabla}_z(I_d(0,z))\right]_{\min}}{I_d(0,z_{\min})} \tag{A5}$$

$z_{\min}$ is the longitudinal position where the ratio $F_{grad}/(KF_{scat})$ is the minimum, as shown in Figure A2 for the case of a pure Gaussian beam.

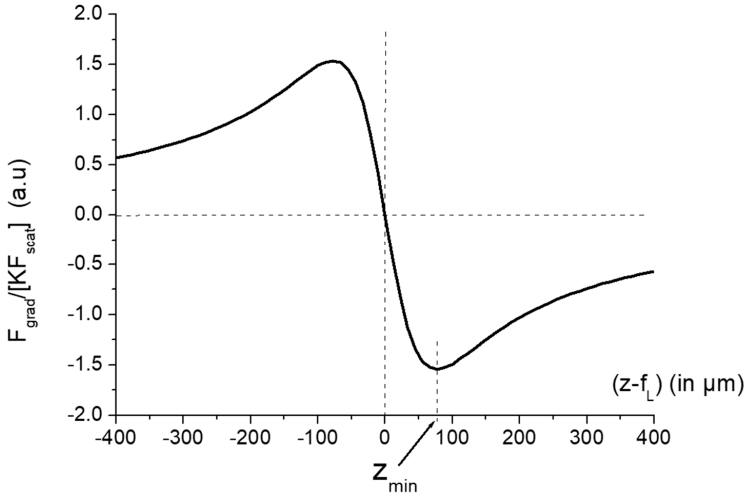

Figure A2. Longitudinal variations of the normalised ratio $F_{grad}/(KF_{scat})$ for a pure Gaussian beam.

Parameter R represents a kind of stability efficiency whose value is important for the operation of the optical trap and can be controlled by the geometry of the laser beam focusing. This point is relevant but is not central to our study since we are rather interested in improving the value of parameter R thanks to the presence of a phase object (PO) set on the path of the incident laser beam. In order to have a simple indicator allowing us to estimate if the PO presence (with PO) improves or not the trap stability compared to the case without the PO (without PO), it is convenient to have recourse to a dimensionless quantity noted Z_L and defined as follows:

$$Z_L = \frac{[R]_{\text{with PO}}}{[R]_{\text{without PO}}} \tag{A6}$$

The longitudinal stability of the trap is observed when the gradient force overcomes the scattering force, thus bringing back the particle pushed by the scattering force so that the particle is trapped. The longitudinal performance of the trap is enhanced (reduced) if the dimensionless factor Z_L is greater (smaller) than unity.

The radial trapping is due to a gradient force proportional to the radial gradient of the intensity. In order to know if the spherical aberration added to the incident beam improves or degrades the radial force, it is convenient to define a radial factor of merit Z_R.

$$Z_R = \frac{\left\{\left|\vec{\nabla}_r I_d(r)\right|_{\max}\right\}^{\text{with PO}}}{\left\{\left|\vec{\nabla}_r I_d(r)\right|_{\max}\right\}^{\text{without PO}}} \tag{A7}$$

$Z_R > 1$ ($Z_R < 1$) means that the presence of the phase object (PO) aberration has improved (degraded) the radial force.

Another parameter noted ${}^{p}Y_R$ defines the radial enhanced factor with respect to the case of an incident Gaussian beam.

$${}^{p}Y_R = \frac{\left\{\left|\vec{\nabla}_r I_d(r)\right|_{\max}\right\}^{\text{with PO}}_{p\geq 1}}{\left\{\left|\vec{\nabla}_r I_d(r)\right|_{\max}\right\}^{\text{p=0}}_{\text{without PO}}} \tag{A8}$$

References

1. Fan, T.Y.; Byer, R.L. Diode laser-pumped solid-state lasers. *IEEE J. Quantum Electron.* **1988**, *24*, 895–912. [CrossRef]
2. Koechner, W. *Solid-State Laser Engineering*, 5th ed.; Springer: Berlin/Heidelberg, Germany, 1999.
3. Hodgson, N.; Weber, H. *Laser Resonators and Beam Propagation*, 2nd ed.; Springer: Berlin/Heidelberg, Germany, 2005.
4. Siegman, A.E. *Lasers*; University Science Books: Herndon, VA, USA, 1986.
5. Allen, L.; Beijersbergen, M.W.; Spreeuw, R.J.C.; Woerdman, J.P. Orbital angular momentum of light and the transformation of Laguerre-Gaussian laser modes. *Phys. Rev. A* **1992**, *45*, 8185–8190. [CrossRef]
6. Pereira, S.F.; Willemsen, M.B.; Van Exter, M.P.; Woerdman, J.P. Pinning of daisy modes in optically pumped verticel-cavity surface-emitting lasers. *Appl. Phys. Lett.* **1998**, *73*, 2239–2241. [CrossRef]
7. Deng, Q.; Deng, H.; Deppe, D.G. Radiation fields from whispering-gallery modes of oxide-confined vertical-cavity surface emitting lasers. *Opt. Lett.* **1997**, *22*, 463–465. [CrossRef]
8. Chen, Y.F.; Lan, Y.P.; Wang, S.C. Generation of Laguerre-Gaussian modes in fiber-coupled laser diode end-pumped lasers. *Appl. Phys. B* **2001**, *72*, 167–170. [CrossRef]
9. Ishaaya, A.A.; Davidson, N.; Machavariani, G.; Hasman, E.; Friesem, A.A. Efficient selection of High-order Laguerre-Gaussian modes in a Q-switched Nd:YAG laser. *IEEE J. Quantum Electron.* **2003**, *9*, 74–82. [CrossRef]
10. Ishaaya, A.A.; Davidson, N.; Friesem, A.A. Very high-order pure Laguerre-Gaussian mode selection in a passive Q-switched Nd:YAG laser. *Opt. Express* **2005**, *13*, 4952–4962. [CrossRef] [PubMed]
11. Rabinovici, R.; Ishaaya, A.A.; Peer, I.; Shimshi, L.; Davidson, N.; Friesem, A.A. Increasing output energy from a passively Q-switched Ar:glass laser. *Appl. Opt.* **2007**, *46*, 7426–7431. [CrossRef]
12. Senatsky, Y.; Bisson, J.F.; Li, J.; Shirakawa, A.; Thirugnansambandam, M.; Ueda, K.I. Laguerre-Gaussian modes selection in diode-pumped solid-state lasers. *Opt. Rev.* **2012**, *19*, 201–221. [CrossRef]

13. Ngcobo, S.; Ait-Ameur, K.; Passilly, N.; Hasnaoui, A.; Forbes, A. Exciting higher-order radial Laguerre-Gaussian modes in a diode-pumped solid-state laser resonator. *Appl. Opt.* **2013**, *52*, 2093–2101. [CrossRef]
14. Hasnaoui, A.; Bencheikh, A.; Ait-Ameur, K. Tailored TEM_{p0} beams for large size 3-D laser prototyping. *Opt. Las. Eng.* **2011**, *49*, 248–251. [CrossRef]
15. Haddadi, S.; Ait-Ameur, K. Improvement of optical trapping effect by structuring the illuminated laser beam. *Optik* **2022**, *251*, 168439. [CrossRef]
16. Siegman, A.E. New developments in laser resonators. In *Optical Resonators*; SPIE: Bellingham, WA, USA, 1990; Volume 1224, pp. 2–14.
17. Born, M.; Wolf, E. *Principles of Optics*, 6th ed.; Pergamon: Oxford, UK, 1980; Chapter 8.
18. Hall, D.R.; Jackson, P.E. *The Physics and Technology of Laser Resonators*; Institute of Physics Publishing: Bristol, UK, 1989; Chapter 9.
19. Passilly, N.; Martel, G.; Ait-Ameur, K. Beam propagation factor of truncated Laguerre-Gauss beams. *J. Mod. Opt.* **2004**, *51*, 2279–2286.
20. Glaze, J. High energy glass lasers. *Opt. Eng.* **1976**, *15*, 136–142. [CrossRef]
21. Bliss, E.S.; Hunt, J.T.; Renard, P.A.; Sommargren, G.E.; Weaver, H.J. Effects of nonlinear propagation on laser focusing properties. *IEEE J. Quantum Electron.* **1976**, *12*, 402–406. [CrossRef]
22. Khoo, I.C.; Hou, J.Y.; Yan, T.H.; Michael, R.R.; Finn, G.M. Transverse self-phase modulation and bistability in the transmission of a laser beam through a nonlinear thin film. *JOSA B* **1987**, *4*, 886–891. [CrossRef]
23. Marburger, J.H. Self-focusing:theory. *Prog. Quantum Electron.* **1975**, *4*, 35–110. [CrossRef]
24. Simmons, W.W.; Hunt, J.T.; Warren, W.E. Light propagation through large laser systems. *IEEE J. Quantum Electron.* **1981**, *17*, 1727–1744. [CrossRef]
25. Holzrichter, J.F.; Speck, D.R. Laser focusing limitations from nonlinear beam instabilities. *J. Appl. Phys.* **1976**, *47*, 2459–2461. [CrossRef]
26. Kelley, P.L. Self-focusing of optical beams. *Phys. Rev. Lett.* **1965**, *15*, 1005–1008. [CrossRef]
27. Hasnaoui, A.; Fromager, M.; Aït-Ameur, K. About the validity of the parabolic approximation in Kerr lensing effect. *Optik* **2019**, *193*, 162986. [CrossRef]
28. Hermann, J. Beam propagation and optical power limiting with nonlinear media. *J. Opt. Soc. Am. B* **1984**, *1*, 729–736. [CrossRef]
29. Hermann, J. External self-focusing, self-bending and optical limiting with thin non-linear media. *Opt. Quantum Electron.* **1987**, *19*, 169–178. [CrossRef]
30. Hunt, J.T.; Renard, P.A.; Nelson, R.G. Focusing properties of an aberrated laser beam. *Appl. Opt.* **1976**, *15*, 1458–1464. [CrossRef]
31. Alda, J.; Alonso, J.; Bernabeu, E. Characterization of aberrated laser beams. *JOSA A* **1997**, *14*, 2737–2747. [CrossRef]
32. Mezouari, S.; Harvey, A.R. Phase pupil functions for reduction of defocus and spherical aberrations. *Opt. Lett.* **2003**, *28*, 771–773. [CrossRef]
33. Boyd, R.W.; Lukishova, S.G.; Shen, Y.R. *Self-Focusing: Past and Present, Fundamentals and Prospects*; Springer: Berlin/Heidelberg, Germany, 2009; Volume 114.
34. Habchi, A.; Harfouche, A.; Hasnaoui, A.; Ait-Ameur, K. A laser weakening the protective capacity of optical limiting devices. *Appl. Phys. B* **2022**, *128*, 14. [CrossRef]
35. Hasnaoui, A.; Fromager, M.; Cagniot, E.; Ait-Ameur, K. Structuring a laser beam subject to optical Kerr effect for improving its focusing properties. *Appl. Phys. B* **2021**, *127*, 75. [CrossRef]
36. Soileau, M.; Williams, W.; Van Stryland, E. Optical power limiter with picosecond response time. *IEEE J. Quantum Electron.* **1983**, *19*, 731–735. [CrossRef]
37. Hermann, J. Simple model for a passive optical power limiter. *Opt. Acta* **1985**, *32*, 541–547. [CrossRef]
38. Sheik-Bahae, M.; Said, A.; Hagan, D.; Soileau, M.; Van Stryland, E. Simple analysis and geometric optimization of a passive optical limiter based on internal self-action. In *Materials for Optical Switches, Isolators, and Limiters*; SPIE: Bellingham, WA, USA, 1989; Volume 1105, pp. 146–153.
39. Hermann, J. Self-focusing effects and applications using thin nonlinear media. *Int. J. Nonlinear Opt. Phys. Mat.* **1992**, *1*, 541–561. [CrossRef]
40. Hermann, J.; Wilson, P. Factors affecting optical limiting and scanning with thin nonlinear samples. *Int. J. Nonlinear Opt. Phys. Mat.* **1993**, *2*, 613–629. [CrossRef]
41. Nalwa, H.S. (Ed.) Handbook of Advanced Electronics and Photonics Materials and Devices. In *Nonlinear Optical Materials*; Academic Press: Cambridge, MA, USA, 2001; Volume 9, Chapter 8.
42. Vivien, L.; Lançon, P.; Riehl, D.; Hache, F.; Anglaret, E. Carbon nanotubes for optical limiting. *Carbon* **2002**, *40*, 1789–1792. [CrossRef]
43. Gao, Y.; Chang, Q.; Ye, H.; Jiao, W.; Li, Y.; Wang, Y.; Song, Y.; Zhu, D. Size effect of optical limiting in gold nanoparticles. *Chem. Phys.* **2007**, *336*, 99–102. [CrossRef]
44. Stepanov, A.L. Nonlinear optical properties of implanted metal nanoparticles in various transparent matrixes: A review. *Rev. Adv. Mater. Sci.* **2011**, *27*, 115–145.
45. Dini, D.; Calvete, M.; Hanack, M. Nonlinear materials for the smart filtering of optical radiation. *Chem. Rev.* **2016**, *116*, 13043–13233. [CrossRef] [PubMed]
46. Muller, O.; Pichot, V.; Merlat, L.; Spitzer, D. Optical limiting properties of surface functionalized nanodiamonds probed by Z-scan method. *Sci. Rep.* **2019**, *9*, 519. [CrossRef] [PubMed]
47. Francois, L.; Mostafavi, M.; Belloni, J.; Delouis, J.F.; Delaire, J.; Feneyrou, P. Optical limitation induced by gold clusters. 1. Size Effect. *J. Phys. Chem. B* **2000**, *104*, 6133–6137. [CrossRef]
48. Hasnaoui, A.; Ait-Ameur, K. Simple modelling of nonlinear losses induced by Kerr lensing effect. *Appl. Phys. B* **2021**, *127*, 100. [CrossRef]

49. Yoshida, A.; Asakura, T. Propagation and focusing of Gaussian laser beams beyond conventional diffraction limit. *Opt. Commun.* **1996**, *123*, 694–704. [CrossRef]
50. Pu, J.; Zhang, H. Intensity distribution of Gaussian beams focused by a lens with spherical aberration. *Opt. Commun.* **1998**, *151*, 331–338. [CrossRef]
51. Furlan, W.D.; Saavedra, G.; Sylvestre, E.; Martinez-Corral, M. On-axis irradiance for spherically aberrated optical systems with obscured rectangular apertures: A study using the Wigner function. *J. Mod. Opt.* **1998**, *45*, 69–77. [CrossRef]
52. Trappe, N.; Murphy, J.A.; Withington, S. The Gaussian beam mode analysis of classical phase aberrations in diffraction-limited optical systems. *Eur. J. Phys.* **2003**, *24*, 403–412. [CrossRef]
53. Hasnaoui, A.; Bencheikh, A.; Fromager, M.; Cagniot, E.; AIt-Ameur, K. Creation of a sharper focus by using a rectified TEM_{p0} beam. *Opt. Commun.* **2011**, *284*, 1331–1334, Erratum in *Opt. Commun.* **2011**, *284*, 4107. [CrossRef]
54. Chai, H.S.; Wang, L.G. Improvement of optical trapping effect by using the focused high-order Laguerre-Gaussian beams. *Micron* **2012**, *43*, 887–892. [CrossRef] [PubMed]
55. Ait-Ameur, K.; Hasnaoui, A. Improving the longitudinal and radial forces of optical tweezers: A numerical study. *Opt. Commun.* **2024**, *551*, 130033. [CrossRef]
56. Haddadi, S.; Hasnaoui, A.; Fromager, M.; Louhibi, D.; Harfouche, A.; Cagniot, E.; Ait-Ameur, K. Use of a diaphragm for transforming a LG_{10} beam into a Flat-Top. *Optik* **2016**, *127*, 2207–2211. [CrossRef]
57. Hasnaoui, A.; Haddadi, S.; Fromager, M.; Louhibi, D.; Harfouche, A.; Cagniot, E.; Ait-Ameur, K. Transformation of a LG_{10} beam into an optical bottle beam. *Las. Phys.* **2015**, *25*, 085004. [CrossRef]
58. Chaloupska, J.; Meyerhofer, D. Characterization of a tunable single-beam ponderative-optical trap. *J. Opt. Soc. Am. B* **2000**, *17*, 713–722. [CrossRef]
59. Ashkin, A. Trapping of atoms by resonance radiation pressure. *Phys. Rev. Lett.* **1978**, *40*, 729–732. [CrossRef]
60. Rhodes, D.P.; Lancaster, G.P.; Livesey, J.; McGloin, D.; Arlt, J.; Dholakia, K. Guiding a cold atomic beam along a co-propagating and oblique hollow light guide. *Opt. Commun.* **2002**, *214*, 247–254. [CrossRef]
61. Wang, Z.; Dai, M.; Yin, J. Atomic (or molecular) guiding using a blue-detuned doughnut mode in a hollow mettalic waveguide. *Opt. Express* **2005**, *13*, 8406–8423. [CrossRef]
62. Dienerowitz, M.; Mazilu, M.; Reece, P.J.; Krauss, T.F.; Dholakia, K. Optical vortex trap for resonant confinement of metal nanoparticles. *Opt. Express* **2008**, *16*, 4991–4999. [CrossRef]
63. Zhan, Q. Trapping mettalic particles with radial polarization. *Opt. Express* **2004**, *12*, 3377–3382. [CrossRef]
64. Zhang, W.; Huang, L.; Santschi, C.; Martin, O.J. Trapping and sensing 10 nm metal nanoparticles using plasmonic dipole antennas. *Nano Lett.* **2010**, *10*, 1006–1011. [CrossRef]
65. Yan, Z.; Pelton, M.; Vigderman, L.; Zubarev, E.R.; Scherer, N.F. Why single-beam optical tweezers trap gold nanowires in three-dimensions. *Acs Nano* **2013**, *7*, 8794–8800. [CrossRef] [PubMed]
66. Rubinsztein-Dunlop, H.; Nieminen, T.A.; Friese, M.E.; Heckenberg, N.R. Optical trapping of absorbing particles. *Adv. Quantum Chem.* **1998**, *30*, 469–492.
67. Lehmuskero, A.; Johansson, P.; Rubinsztein-Dunlop, H.; Tong, L.; Käll, M. Laser trapping of colloidal metal nanoparticles. *Acs Nano* **2015**, *4*, 3453–3469. [CrossRef] [PubMed]
68. Gongjian, Z.; Man, Z.; Yang, Z. Wave front control with SLM and simulation of light wave diffraction. *Opt. Express* **2018**, *26*, 33543. [CrossRef] [PubMed]
69. Jewel, A.R.; Akondi, V.; Vohnsen, B. A direct comparison between a MEMS deformable mirror and a liquid crystal spatial light modulator in signal-based wavefront sensing. *J. Eur. Opt. Soc. Rapid Publ.* **2013**, *8*, 13073. [CrossRef]
70. Cagniot, E.; Fromager, M.; Godin, T.; Passilly, N.; Brunel, M.; Ait-Ameur, K. Variant of the method of Fox and Li dedicated to intracavity laser beam shaping. *JOSA A* **2011**, *28*, 489–495. [CrossRef] [PubMed]
71. Harrison, J.; Forbes, A.; Naidoo, D. Amplification of higher-order Laguerre-Gaussian modes using a dual-pass MOPA system. *Opt. Express* **2023**, *31*, 17408–17423. [CrossRef] [PubMed]
72. Sheppard, C.J.R.; Porras, M.A. Comparison between the propagation properties of Bessel-Gauss and generalised Laguerre-Gauss beams. *Photonics* **2023**, *10*, 1011. [CrossRef]
73. Khonina, S.N.; Ustinov, A.V.; Kharitonov, S.I.; Fomchenkov, S.A.; Porfirev, A.P. Optical bottle shaping using axicons with amplitude or phase apodization. *Photonics* **2023**, *10*, 200. [CrossRef]
74. Neuman, K.; Block, S. Optical trapping. *Rev. Sci. Instrum.* **2004**, *75*, 2787–2809. [CrossRef]
75. Ashkin, A. Acceleration and trapping of particles by radiation pressure. *Phys. Rev. Lett.* **1970**, *24*, 156–159. [CrossRef]
76. Ashkin, A.; Dziedzic, J.M. Optical levitation by radiation pressure. *Appl. Phys. Lett.* **1971**, *19*, 282–285. [CrossRef]
77. Harada, Y.; Asakura, T. Radiation forces on a dielectric sphere in the Rayleigh scattering regime. *Opt. Commun.* **1936**, *124*, 529–541. [CrossRef]
78. Lang, M.J.; Block, S.M. Resource Letter: LBOT-1: Laser-based optical tweezers. *Am. J. Phys.* **2003**, *71*, 201–215. [CrossRef]
79. Dienerowitz, M.; Mazilu, M.; Dholakia, K. Optical manipulation of nanoparticles: A review. *J. Nanophotonics* **2008**, *2*, 021875. [CrossRef]